博士論文

Behavioral state- and olfactory sensory input-dependent regulation of life/death decision and dendritic morphology of adult-born granule cells in the olfactory bulb

（行動様式と嗅覚入力による嗅球新生顆粒細胞の生死及び樹状突起形態の調節）

持丸　大輔

TABLE OF CONTENTS

Abstract	**1**
Introduction	**3**
Materials and Methods	**8**
Results	**20**
Discussion	**33**
Acknowledgements	**45**
References	**46**
Figure Legends	**57**
Figures	**62**

Abstract

Granule cells (GCs) in the olfactory bulb (OB) continue to be generated in adulthood. Nearly half of adult-born GCs are incorporated to the OB circuitry, while the others eliminated. Previous studies have shown that olfactory sensory inputs influence greatly survival and death decision of adult-born GCs. However, it is not known whether the regulation occurs in local areas of the OB. In addition, it is not known whether the survival and death decision occurs in association with specific behaviors of animals. By using mice which lack olfactory sensory inputs to a restricted OB domain, I showed that lack of local sensory inputs greatly reduced survival of adult-born GCs in the local OB domain. Under restricted feeding, enhanced GCs death in the local OB domain occurred during postprandial (after-meal) period. These results indicated that local sensory inputs regulate survival and death decision of adult-born GCs in the local OB domain during postprandial period.

Next I examined how morphological development of adult-born GC dendrites is regulated by olfactory sensory inputs. In the OBs which are deprived of olfactory sensory inputs with nostril occlusion, arborization and protrusion formation of

adult-born GC dendrites in different OB layers drastically changed. This result indicates that development of adult-born GC dendrites is heavily dependent on sensory inputs.

Introduction

The olfactory bulb (OB) is a highly plastic neuronal circuitry in the adult mammalian brain. Granule cells (GCs), inhibitory interneurons in the OB, are generated and incorporated into the neuronal circuitry from the embryonic stage right through into adulthood (Lledo et al., 2006; Lois and Alvarez-Buylla, 1994; Luskin, 1993). GCs are generated at the subventricular zone (SVZ) and migrate tangentially to the OB through the rostral migrate stream (RMS) (Figure 1). About seven days after generation, GCs reach the core region of the OB and start radial migration to the granule cell layer (GCL) in the OB. Then they extend dendrites and make dendrodendritic synapses with lateral dendrites of mitral/tufted cells, the projection neurons in the OB, in the external plexiform layer (EPL). GCs also make synapses with somata of mitral cells in the mitral cell layer (MCL). Synaptogenesis of adult-born GCs in these layers extensively occurs from 14 to 28 days after their generation (Carleton et al., 2003; Kelsch et al., 2008; Petreanu and Alvarez-Buylla, 2002; Whitman and Greer, 2007).

Among adult-born GCs, approximately half are incorporated into the preexisting neuronal circuitry while the remainder are eliminated by apoptosis (Petreanu and

Alvarez-Buylla, 2002; Rochefort et al., 2002; Yamaguchi and Mori, 2005). This selection process is crucial for proper function of adult OB. When apoptotic elimination of adult-born neurons is suppressed by a caspase inhibitor, odor discrimination ability is disturbed (Mouret et al, 2009), presumably because of the presence of inappropriately incorporated adult-born GCs.

Survival rate of adult-born GCs is regulated by olfactory sensory experience. For example, enrichment of odor experiment and odor discrimination task increases survival rate of adult-born GCs (Petreanu and Alvarez-Buylla, 2002; Rochefort et al., 2002). On the other hand, olfactory sensory input deprivation greatly reduces the survival rate of adult-born GCs (Petreanu and Alvarez-Buylla, 2002; Fiske and Brunjes, 2001; Yamaguchi and Mori, 2005). Olfactory sensory experience-dependent survival and death decision of new GCs is promoted in a specific time period after their generation. Olfactory sensory inputs during days 14-28 after generation of new GCs strongly influence their survival rate (Yamaguchi and Mori, 2005). This critical period corresponds to the period of synaptic formation of adult-born GCs with preexisting neurons, suggesting the crucial role of synaptic inputs to new GCs for their survival and

death decision.

However, neuronal mechanisms of how olfactory sensory inputs regulate the survival and death of new GCs are not well understood. One of the reasons for the difficulty in addressing this question has been the lack of appropriate method of selective ablation of olfactory sensory inputs to a local region of the OB. For example, in previous studies, manipulation of olfactory inputs have been conducted in the entire OB. Odor stimulation using various kinds of odors typically activates entire OB. Odor deprivation by nostril occlusion or knockout of signaling molecules suppress the activity of olfactory sensory inputs to entire OB.

Another interesting question is whether the time window of the survival and death decision of new GCs is linked with specific behavioral states of animals. The synaptic plasticity underlying learning and memory is crucially regulated by the wake-sleep cycle. In the hippocampus and neocortex, experience-induced neuronal activity occurs during waking states, while neuronal activity during subsequent sleep is thought to facilitate the consolidation of experience-based memories and promote the concomitant reorganization of neuronal circuits (Buzsaki, 1989; Diekelmann and Born, 2010). In the

present study, I addressed the question of whether the selection of adult-born GCs occurs in association with specific behaviors.

For this purpose, I utilized gene-manipulated mice that lack olfactory sensory inputs in a specific domain in the OB (Kobayakawa et al., 2007). In the mice, olfactory sensory neurons that are targeted to the dorsal domain (D-domain) of the OB were selectively ablated. These mice are therefore referred to as ΔD mice. Using the ΔD mice, I found that olfactory sensory inputs to local OB domain regulate the survival and death of new GCs in the domain. Further, I found that, in the ΔD mice, enhanced death of GCs during postprandial sleep (Yokoyama et al., 2011) is more prominent in the sensory input-deprived D-domain compared with that in the sensory input-intact V-domain. These observations suggest that local olfactory sensory inputs during eating result in the survival and death decision of new GCs in the local OB domain during the subsequent post-behavioral period.

Given these results, I further addressed the question of how the development of dendritic structures of newly-generated adult-born GCs is regulated by olfactory sensory inputs. GC dendrites contact to the lateral dendrites of mitral/tufted cells in the

EPL, and contact to the somata of mitral cells in the MCL. GCs receive olfactory sensory inputs via the mitral/tufted-to-granule excitatory synapses in the EPL and MCL. While it has been reported that density of dendritic protrusions of adult-born GCs in the EPL is reduced in the sensory-deprived OB by nostril occlusion (Saghatelyan et al, 2005; Kelsch et al., 2009), possible alteration in the dendritic protrusion density of adult-born GCs in the MCL is not well understood. I therefore examined the morphology of dendritic arborization and dendritic protrusions of newly-generated GCs in the EPL and MCL between olfactory input-intact and -deprived mice. I found that drastic morphological changes of dendritic structures of adult-born GCs in these layers occurred in an olfactory sensory inputs-dependent manner.

Materials and Methods

Animals and housing

C57BL/6 male mice weighing 21-23 g (Nihon-SLC) were used. They were 8 weeks old at the start of the restricted feeding schedule. ΔD male mice (Kobayakawa et al., 2007) aged 11-12 weeks and age-matched C57BL/6 male mice were used for comparative analysis. To avoid social interaction, they were housed individually in plastic cages (23×17×12 cm), and each cage was kept in an isolation box (Clea Japan). The mice were maintained under a 12-h light-dark cycle, with lights on at 5:00 and off at 17:00. The temperature was set at 25 ℃ at all times. All experiments were conducted in accordance with the guidelines of the Physiological Society of Japan, and were approved by the Experimental Animal Research Committee of the University of Tokyo.

Restricted feeding

To control feeding behavior, restricted feeding conditions were adopted (Mistlberger, 1994; Gooley et al., 2006). Food was supplied for only 4 hours per day. In most experiments, food was supplied from 11:00 to 15:00. After 9 days of habituation to the

feeding schedule, the animals were analyzed at various circadian time points on day 10. Water was available *ad libitum* at all times. Within 9 days of habituation to the protocol, the body weight of mice declined to 87.9% on average of that just before the start of food restriction. After habituation, individual mice ate an average of 3.3 g of food pellets during the 4 hours of food supply.

Behavioral analysis and disturbance of postprandial behaviors

Animal behavior around the feeding and postprandial period was recorded with a digital video camera and analyzed with the help of SMART software (PanLab). Behavior was categorized as eating, drinking, grooming, exploratory behavior (including sniffing, digging, and locomotor activity), or resting/sleeping. Behaviors that lasted longer than 5 sec were evaluated and charted on a graph. Combined histograms of each type of behavior were created using Gantt chart software from Gansuke (Shareware, Japan; downloaded from http://www.gansuke.com/). Postprandial behaviors were disrupted by a gentle handling method previously used for sleep deprivation experiments (Mistlberger et al., 2003). When mice started to rest, sleep, or show an extended period

of grooming (more than 5 sec) during the feeding and postprandial period, they were stimulated by gently stroking the body with the flat side of a soft plastic ruler, while their eating, drinking and exploratory behaviors were not disturbed. This procedure successfully prevented resting, sleeping, and sustained grooming during the period in most of the examined mice. The procedure did not reduce the amount of food consumed during the feeding and postprandial period in every analysis of the present study.

Olfactory sensory deprivation by plug insertion

To induce olfactory sensory deprivation, mice were anesthetized lightly with diethyl ether on the day prior to the beginning of the restricted feeding schedule, and a plug into one nostril. Plugs were made by polyethylene tube (SP30, Natsume) filled with silk (ELP No. 4, Natsume) and with adhesion bond. The effectiveness of nostril occlusion was confirmed by remaining the plug in the nostril at the day of perfusion fix.

BrdU labeling

For the analysis of long-term survival of adult-born GCs in ΔD and wild-type mice,

they were injected intraperitoneally with BrdU for 5 consecutive days (100 mg/kg each, one injection per day) and analyzed 9, 14, 28 and 56 days after the last day of BrdU injection (Figure 4). In experiment of Figure 7, ΔD mice were injected intraperitoneally with BrdU for 7 consecutive days (100 mg/kg each, two injections per day).

Immunohistochemistry

Mice were deeply anesthetized by intraperitoneal injection of sodium pentobarbital (50 mg/kg) and transcardially perfused with ice-cold 4% paraformaldehyde (PFA). Serial coronal cryosections of the OB (20 or 50 μm thickness) were prepared from the rostral tip to the caudal end. Immunohistochemical analysis was performed as described previously (Yamaguchi and Mori, 2005). The primary antibodies used were: rabbit anti-cleaved caspase-3 antibody (Cell Signaling Technology, 1:100 dilution), rat anti-BrdU antibody (Oxford Biotechnology, 1:100 dilution), goat anti-DCX antibody (against C-terminus; Santa Cruz Biotechnology, 1:100 dilution), rabbit-anti-OCAM antibody (Yoshihara et al., 1997, 1:1000 dilution), mouse anti-NeuN antibody (millipore, 1:200 dilution), rabbit anti-c-fos antibody (Santa Cruz Biotechnology, 1:1000 dilution)

and rat anti-GFP antibody (Nakarai Tesque, 1:200 dilution). Secondary antibodies were Alexa Fluor 488-, 546-, or 647-conjugated antibodies (Molecular Probes, 1:300 dilution). Sections were incubated with appropriate antibodies, and the nuclei were stained with DAPI. For BrdU detection, sections were incubated with 0.025 N HCl for 30 min at 65 °C, rinsed with 0.1 M boric acid (pH 8.5), and subjected to immunohistochemical analysis. The sections were examined under a fluorescence microscope (Leica) or a confocal laser scanning microscope (Leica).

TUNEL assay

PFA-fixed brain samples were cryosectioned to a 20 μm thickness. The samples were postfixed with ethanol/acetate (2:1) for 5 min at -30 °C and subject to TUNEL assay (MEBSTAIN apoptosis kit II, MBL) according to the manufacturer's instructions. For TUNEL staining, 20 μm thick sections were used and were incubated with proteinase-K (10 μg/ml in PBS) for 15 min at room temperature after postfixation with ethanol/acetate.

Cell counting

Coronal sections of the OB from the rostral tip to the caudal end were selected at the rate of 1 in every 10 serial sections. For the analysis of neonate-born GCs in the OB, 5 of 10 serial sections were analyzed. Active caspase-3-labeled GCs in the GCL were counted under the fluorescence microscope at x200 magnification, and the numbers were added and then multiplied by 10 to estimate the total number of labeled GCs per OB. For comparative analysis of ΔD mouse and wild-type mouse OBs, coronal sections at the central portion in the rostro-caudal axis were used, which included a considerable volume of both D- and V-domains. D- and V-domains were determined by OCAM expression (Yoshihara et al., 1997) in the glomeruli and the volume of D- and V-domains in each section was calculated using Metamorph software (Universal Imaging Corporation). The density of caspase-3-activated or BrdU-labeled GCs in each domain was then determined.

To quantify the total number of BrdU-labeled cells in the OB, coronal OB sections were selected at the rate of 1 in every 30 serial sections, and labeled cells in the selected sections were counted, summed, and multiplied by 30. We confirmed that the obtained

data were not significantly different from the data obtained by analyzing OB sections at the rate of 1 in every 10 serial sections.

Odor stimulation

ΔD and wild-type male mice were housed individually in isolation boxes and supplied with pure air that was deodorized through charcoal filter. The mice were kept in new shavings without food pellets for 6 hours before odor application. Propionic acid was diluted to 1/5 concentration with mineral oil, and a cotton sheet soaked with 50 μl of the diluted solution was put in a stainless tea ball. Odor was applied by placing the tea ball on the cage top for 5 min three times at 5-min intervals. At 1 hour after the last odor application, the mice were perfusion-fixed and subjected to the analysis of c-fos expression in the OB.

Virus preparations

Adult-born GCs in ΔD mice and their control wild-type mice were labeled by EGFP (enhanced green fluorescent protein)-expressing retrovirus. Retrovirus encoding EGFP

have vesicular stomatitis virus-G (VSV-G) envelop (kindly provided Dr. Mochizuki, H., University of Kitasato, Japan, Suzuki et al., 2002).

In other experiments using wild-type mice, adult-born GCs were labeled by EGFP-expressing lentivirus. For sensory input-intact mice, an EGFP-expressing vector pCL20c-CMV-EGFP-WPRE was used. For the generation of this vector, the ClaI-digested WPRE fragment from CSII-CMV-MCS (kindly provided by Dr. H. Miyoshi, RIKEN BioResource Center, Ibaraki, Japan, Miyoshi et al., 1998) was inserted into the ClaI site of pCL20c-EF1α-EGFP (kindly provided by Dr. Arthur W. Nienhuis, St. Jude Children's Research Hospital, TN, USA, Hanawa et al., 2004). Then the BglII/HindIII-digested cytomegalovirus immediate-early enhancer/promoter (CMV) fragment from pCMVTNT (promega, USA) was inserted into MluI/SmaI-digested pCL20c-EF1α-EGFP-WPRE to replace EF1α promoter sequence.

Lentivirus was produced by co-transfection with a mixture of four plasmids for HEK293T cells using the calcium phosphate transfection method. The four plasmid mixture consisted of pCAGkGP1.1R, pCAG4RTR2, pCAG-VSV-G (kindly provided by Dr. Arthur W. Nienhuis, St. Jude Children's Research Hospital, TN, USA), and

pCL20c-CMV-EGFP-WPRE. The medium containing lentivirus was cleared by low-speed centrifugation and filtered using a 0.22 μm pored membrane. Then medium was centrifuged at 12,500 rpm, 4 °C, 8 hours. After centrifugation, lentivirus pellets were resuspended with 50-100 μm of 4 °C PBS (x800-1600 concentration from medium).

For sensory-deprived mice by nostril occlusion, another EGFP-expressing lentivirus vector CS-CDF-EG-PRE, containing EF1α promoter, WPRE and EGFP cDNA, was used (kindly provided by Dr. H. Miyoshi, RIKEN BioResource Center, Ibaraki, Japan). CS-CDF-EG-PRE, pCAG-HIVgp, and pCMV-VSV-G-RSV (also provided by Dr. Miyoshi) were co-transfected to HEK293T cells and generated lentivirus were collected by the same methods described above.

Virus injection

The mice were deeply anesthetized with ketamine (50 mg/kg) after pre-anesthesia with medetomidine and atropine, and were mounted in a stereotaxic apparatus (SR-5N, Narishige). Body temperature was maintained at 37.5 °C by animal blanket controller

(ATB-1100, Nihon Kohden).

For retrovirus injection, a grass pipette whose tip diameter was 50-60 μm was inserted at the SVZ (anterior: 0.0 mm, lateral: 1.7 mm from the bregma) and retrovirus solution (0.4 μl) was injected five points (depth: 1.8, 2.0, 2.2, 2.4 and 2.6 mm from the dorsal surface) by microprocessor-controlled syringe pump (IC3200, Kd Scientific). The injection rate was 0.4 μl/min.

For lentivirus injection, a grass pipette whose tip diameter was 75-90 μm was inserted at the RMS. Distance from the bregma to the blood vessel at the boundary between the OB and neocortex was measured and x0.71 of that distance from the bregma was set as the anteroposterior axis of the injection point. The injection was made at 0.82 mm lateral from the center with 2.85 mm deep from the dorsal surface. Lentivirus solution (0.2 μl) was injected by microprocessor (Micro4, WPI)-controlled syringe pump (UltraMicroPump II, WPI). The injection rate was 0.1 μl/min.

Image acquisition and morphological analysis of EGFP-expressing adult-born GCs

Immnohistcamical stained OB coronal sections (thickness: 50 μm) were mounted on

slide grass with mounting medium (ProLong Gold, life technologies) and cover glass (thickness: 0.12-0.17 mm). Images of EGFP-expressed adult-born GCs were taken by confocal laser scanning under oil-immersion x63 objective lens (NA=1.4) with LAS AF software (SP-5, Leica) (scanning speed was 100 Hz and line average was twice). Images of one X-Y plane were acquired 1024x1024 pixels with x4 electrical zoom. Pixel size was 0.06 x 0.06 μm and z-step was 0.4 μm. Length of dendrites and diameter of dendritic protrusions were measured in the one X-Y plane of Z-stacked confocal image using LAS AF.

To observe similar cell population across different animals as possible, I consistently analyzed GFP-labeled cells at day 14 after the labeling. I observed GFP-labeled cells in an OCAM-negative dorsal domain at the middle portion (along rostro-caudal axis) of the OB. Further, because GCs can be roughly classified into mitral cell-targeting and tufted cell-targeting GCs, I chose presumed mitral cell-targeting GCs for analysis, whose dendrites start to bifurcate within the mitral cell layer (MCL), a layer deep to the external plexiform layer (EPL) (Mori, 1987). All the acquired images were randomly numbered and were subjected to blind analysis.

Statistical analysis

For statistical analysis, the two-tailed unpaired or paired *t*-test was used for groups of two, while one-way ANOVA with the post-hoc Bonferroni test was used for multiple comparisons. Statistical significance was set at $p = 0.05$.

Results

Mice depleted with olfactory sensory neuron in the dorsal zone of the olfactory epithelium lack glomeruli in the dorsal domain of the OB

Do olfactory sensory inputs to local OB areas regulate the survival and death of adult-born GCs in the local OB areas? To address this question, I used ΔD mice, in which olfactory sensory neurons (OSNs) in the dorsal zone (D-zone) of the olfactory epithelium were genetically ablated (Figure 2A) (Kobayakawa et al., 2007). In wild-type (WT) mice, OSNs of D-zone project to dorsal domain (D-domain) of the OB and form glomeruli in the D-domain. However, the OB of ΔD mice lacked glomeruli in the D-domain due to depletion of D-zone OSNs (Figure 2A,B), as reported previously (Kobayakawa et al., 2007). In WT mice, OSNs in the ventral zone (V-zone) of the epithelium express a cell adhesion molecule OCAM, while OSNs in the D-zone do not (Yoshihara et al., 1997). Accordingly, glomeruli in the V-domain are OCAM-positive (Figure 2B; WT, arrow) and those in the D-domain are OCAM-negative (Figure 2B; WT, arrowhead) (Yoshihara et al., 1997, Matsumoto et al., 2010). In the ΔD mice OB, all the glomeruli were OCAM-positive (Figure 2B; ΔD, arrow) and OCAM-negative

glomeruli were lacking. I therefore defined the glomeruli-lacking domain in the ΔD mice OB as D-domain and OCAM-positive glomeruli-covering domain as V-domain. Figure 2C shows unrolled glomerular maps of ΔD and WT mouse OBs, which are reconstructed from OB coronal sections. Following quantitative analyses of incorporation and death of adult-born GCs were conducted in coronal sections at the central portion the rostrocaudal axis of ΔD and WT mouse OBs, which include a considerable volume of both D- and V-domain (Figure 2C, ★).

Reduced activity of GCs in the D-domain of ΔD mice OB following odor stimulation

GCs activated by odor stimulation express an immediate early gene, c-fos (Magavi et al., 2005). I compared c-fos expression in the ΔD and WT mouse OB following odor stimulation with propionic acid application. As expected, a large number of GCs in the D-domain of WT mouse OB expressed c-fos (Figure 3). On the other hand, c-fos expression in GCs in the D-domain of ΔD mouse OB was drastically reduced. This result indicates that GCs in the D-domain of ΔD mouse OB are not appropriately

activated by olfactory sensory inputs.

Immature adult-born GCs accumulate in the D-domain of the ΔD mouse OB in high density, but their long-term survival rate is reduced

Deprivation of olfactory sensory inputs by nostril occlusion drastically reduces the survival of adult-born GCs (Yamaguchi and Mori, 2005). To examine whether sensory deprivation in the local OB area influences survival of adult-born GCs only in the local OB area or whole OB area, I labeled adult-born GCs with systemic BrdU injection for 5 consecutive days in the ΔD mice and WT mice, and analyzed BrdU-positive GC density in each of the D- and V-domain at days 9, 14, 28 and 56 after the last BrdU injection. It has been shown that most BrdU-positive cells in the GCL of the OB are NeuN-expressing GCs (Yamaguchi and Mori, 2005). On days 9-13 after the BrdU-labeling, labeled new GCs accumulated in higher density (1.7-fold) in the D-domain than in V-domain of the ΔD mouse OB (Figure 4A,B). However, the density in the D-domain remarkably reduced by days 28-32, and became comparable to that in the V-domain at days 28-32 and days 56-60 (Figure 4A,B,D). Long-term survival rate of

adult-born GCs (ratio of BrdU positive cell number; at days 56-60 versus at days 9-13) in the D- domain of ΔD mouse was 34.7%, which was significantly lower than that in the V-domain (62.3%; Figure 4E).

In the WT mouse OB, the density of BrdU-labeled GCs in the D-domain of the OB at days 9-13 was slightly higher than that in the V-domain, and the ratio (D-domain / V-domain) was constant across all time points (~1.2; Figures 4A,C,D). Long-term survival rate of adult-born GCs in WT mouse OB was 55.5 % and 52.5 % in the D- and V-domain, respectively, whose value were comparable to that in the V-domain of ΔD mouse OB (Figure 4E). These results indicate that local sensory inputs regulate the recruitment of immature adult-born GCs to the local OB area and survival rate of adult-born GCs in the local OB area. It was rather unexpected that immature new GCs accumulated into D-domain of ΔD mouse OB, because previous studies showed that migration of new GCs into the OB was either unchanged or suppressed for the sensory-deprived OB by nostril occlusion and knockout of cyclic nucleotide-gated channels in the entire OSNs (Petreanu & Alvarez-Buylla, 2002; Saghatelyan et al, 2004; Yamaguchi & Mori, 2005) (see Discussion).

Finally, I counted the number of BrdU-positive cells in the whole OB of WT and ΔD mouse at days 9-13 after BrdU injection (Figure 4F). The number in the ΔD mouse OB was significantly lower than in the WT mouse OB. This observation suggests that higher density of GCs at 9-13 days of age in the D-domain of ΔD mouse OB is not due to the increased generation of a particular subset of new GCs which are destined to migrate into the D-domain.

In the D-domain of ΔD mouse OB, enhancement of GC cell death occurs during postprandial period

Olfactory sensory experience is tightly linked to behavioral states of animals, such as food searching/eating, mating with partners and escaping from predators (Doty 1986). Because many odor-guided behaviors have to be newly acquired or updated to cope with a changing odor world, it is likely that neuronal circuits in the central olfactory system, including the OB, are reorganized on a daily basis during the odor experience and the acquisition/improvement of odor-guided behaviors. I therefore hypothesized that survival and death decision of new GCs may occur in association with

olfaction-related behaviors. Together with the notion in the hippocampus and neocortex that reorganization of the neural circuits that accompanies memory consolidation may occur during the rest/sleep period following learning process during waking (Buzsaki 1989; Diekelmann and Born 2010), I chose feeding behavior for analysis, which is a typical olfactory behavior often followed by rest and sleep.

I conducted food restriction for ΔD and WT mice, in which mice could access food pellets only during 4 hours (11:00-15:00) in a day (Figure 5A). After the habituation to this food restriction paradigm for a week, the mice reproducibly showed extensive food eating and subsequent postprandial behavior (grooming, resting and sleeping) during the period of food delivery. They typically devoted to eating and drinking during the initial 1 hour of food delivery, and then started to show typical postprandial behaviors (see Figure 6A). On day 10 of food restriction, I sampled mice before feeding period (11:00) and after showing feeding and postprandial behaviors (13:00) (Figure 5A), and counted the number of caspase-3-activated apoptotic GCs (Figure 5B). The density of caspase-3-activated GCs in the D-domain of ΔD mouse OB increased 3.2-fold in postprandial period compared with that before feeding, while that in the V-domain

increased 2.2-fold (Figure 5B,C). In the WT mouse OB, the density of caspase-3-activated GCs in the D-domain increased 2.3-fold in postprandial period, while that in the V-domain 2.0-fold (Figure 5D). The ratio of caspase-3-activated GC density in the D-domain of ΔD mouse OB to that in the V-domain of ΔD mouse OB in the postprandial period (D-domain / V-domain) was significantly higher than that before feeding period ($p=0.009$), while that ratio in the WT OB showed no significant difference between the two time points (Figure 5E). These results indicate that the lack of olfactory sensory inputs to the local OB domain greatly enhance the elimination of GCs in that local domain during postprandial period. I further performed TUNEL staining and confirmed the increase in apoptotic GCs death in the D-domain of ΔD mouse OB during postprandial period (Figure 5F).

Enhanced GC elimination in the D-domain of ΔD mouse OB occurs in association with postprandial behavior

Why does the extent of apoptotic GCs death in the D-domain of ΔD mouse OB increase during postprandial period? To address this question, I analyzed the behaviors of ΔD

mouse during the initial 2 hours of food delivery (11:00-13:00) (Figure 6A). ΔD mice showed extensive eating and drinking behavior during initial 1 hour. During the next 1 hour, they showed increase in grooming behavior and rest and sleep behavior. While caspase-3-activated apoptotic GCs showed no significant increase during the initial 1 hour both in the D- and V-domain (Figure 6B,C; No disturb: 1h), apoptotic GCs increased during the next 1 hour, where increase in D-domain was more prominent than in V-domain (No disturb: 2h). When postprandial behaviors were inhibited by gently stimulating the mice's body, enhanced GC apoptosis was suppressed both in the D- and V-domain (Disturb: 2h). This result indicates that enhanced GC apoptosis in the D- and V-domain of ΔD mouse OB occurs in association with postprandial behavior.

A majority of apoptotic GCs in the D- and V-domain of ΔD mouse OB is adult-born new GCs.

To examine whether apoptotic GCs in the ΔD mouse OB are adult-born new GCs, adult-born GCs were labeled by BrdU injection for 7 consecutive days. After 10 days of food restriction, BrdU labeling and expression of doublecortin (DCX), a marker for

immature neurons (Brown et al., 2003), were examined in the caspase-3-activated GCs (Figure 7). More than 50% of caspase-3-activated GCs showed either BrdU labeling (14-20 days of age) or DCX expression both before feeding period and postprandial period in the D-domain as well as in V-domain of ΔD mouse OB (Figure 7). This result indicated that a majority of apoptotic GCs in the D- and V-domain of ΔD mouse OB was adult-born new GCs. From these results, I propose a "two-stage model" for the sensory experience-dependent selection of adult-born new GCs, in which the two stages represent olfactory sensory experience during food search and eating followed by postprandial behaviors including sleep (Figure 8) (see Discussion) (Yokoyama et al. 2011; Yamaguchi et al. 2013).

Lack of local olfactory sensory inputs reduces protrusions on EPL dendrites of adult-born GCs.

How are adult-born new GCs eliminated or incorporated into preexisting OB neuronal circuit in a sensory experience-dependent manner? To address this question, I observed the morphology of dendritic protrusions of new GCs in the ΔD mouse OB. Dendrites of

new GCs make dendrodendritic synaptic contacts with lateral dendrites of mitral/tufted cells in the EPL. Because GCs receive olfactory sensory input via the dendrodendritic synapses in the EPL and sensory deprivation is known to inhibit the development of these synapses (Kelsch et al., 2009), I first examined the dendritic protrusions of new GCs in the EPL of the D-domain of ΔD mice Newly generated GCs were labeled by injecting GFP-expressing retrovirus in the SVZ. After 28 days of ad libitum feeding, the mice were perfusion fixed and the labeled new GCs in the OB were observed. Dendrites of new GCs in the EPL of the D-domain appeared to have a lower density of protrusions than those of the V-domain of the same OB (Figure 9).

Development of dendritic arbors and dendritic protrusions of new GCs in the sensory-input intact and sensory input-deprived OB

Although ΔD mice are the powerful tool in addressing the role of sensory inputs to new GCs, the layer structure of D-domain of ΔD mouse's OB is somewhat perturbed, such that some mitral cell somata are displaced in the EPL. In addition, the boundary between EPL and MCL, where somata of mitral cells are aligned, was difficult to define

unequivocally. So I utilized nostril-occluded wild-type mice to address the role of olfactory sensory input in the development of dendritic structures of new GCs across the MCL and EPL.

I injected EGFP-expressing lentivirus to RMS to label adult-born GCs (Figure 10A). Five days after the injection, a group of mice received unilateral nostril occlusion for olfactory sensory deprivation (Figure 10B). In order to analyze the dendritic morphology of adult-born GCs under the well-controlled behavioral states, the mice were then subjected to restricted feeding and analyzed on day 14 after the lentivirus injection (corresponding to day 10 of restricted feeding). OBs were collected from 4 different time points, 9:00, 11:00, 12:00 and 13:00, when mice showed rest/sleep, exploration in the cage, extensive eating and postprandial rest/sleep, respectively.

Figure 11A shows dendritic arbors of new GCs in the sensory-intact and -deprived OB. Dendritic arbors of new GCs in sensory-deprived OB were remarkably diminished in the EPL. No new GCs in the sensory-deprived OB analyzed had branch points in the EPL (Figure 11B). Instead, new GCs in the sensory-deprived OB had much branch points in the MCL than new GCs in the sensory-intact OB (Figure 11C). In addition,

total dendrite length of new GCs in the sensory-deprived OB became shorter in the EPL and longer in the MCL, than that of new GCs in the sensory-intact OB (Figure 11D,E).

Next, dendritic protrusions in the EPL and MCL were examined. Protrusion density of new GCs of sensory-deprived OB tended to decrease in the EPL but not in the MCL, compared to that of new GCs in the sensory-intact OB (Figure 12A-C). While total protrusion number (density x total dendritic length) of new GCs in sensory input-deprived OB was significantly smaller in the EPL, their total protrusion number in the MCL became larger than that in the sensory-intact OB (Figure 12D,E). Ratio of protrusions in the MCL among total protrusions in the MCL and EPL increased to 70 % for new GCs in the sensory-deprived OB (Figure 12F). These results indicate that contact formation of new GCs to mitral cells in the sensory-deprived OB is biased to the somata rather than the dendrites of mitral cells.

Lastly, sizes of dendritic protrusions of new GCs in the MCL were examined. The size distribution of protrusions in the EPL did not significantly differ between new GCs in the sensory-intact and -deprived OB (Figure 13A,B). In contrast, that in the MCL shifted to the larger side for new GCs in sensory-deprived OB (Figure 13C,D). This

observation is in accord with the hypothesis that new GCs might adapt to reduced neuronal activity in the sensory-deprived OB by making more and larger synaptic contacts to mitral cell somata (see Discussion).

Discussion

Addressing sensory input-dependent mechanisms of survival and death decision of new GCs using ΔD mice

Animals daily encounter various kinds of odor signals. They have to acquire novel odor-guided behaviors to properly behave in the ever-changing odor circumstances. Adult neurogenesis in the OB is considered to provide highly plastic features to the neuronal circuit and contribute to the acquisition, updating and potentiation of odor guided behaviors. To understand this point, it is important how new OB neurons are utilized depending on the olfactory sensory inputs and animals' behaviors. I have examined the survival and death decision and development of dendritic structures of new GCs using olfactory sensory input-manipulated mice.

The most common way of suppressing olfactory inputs is occluding one nostril unilaterally. This manipulation results in a stable and continual olfactory sensory deprivation. However, this is an artificial condition in that sensory input is deprived in the entire ipsilateral OB. Under physiological condition, odor inputs activate a subset of GCs while leaving others inactivated. Effect of olfactory inputs on new GCs had better

be examined under such a mosaic activation of GCs. ΔD mice provide a unique and efficient way of analysis, in which GCs in the different domains in the same OB receive different level of activation by odor inputs. I here compared the fate of new GCs in D- and V-domain of the ΔD mouse OB, which receive little and substantial odor inputs, respectively. Using these mice, I examined whether fate of new GCs in the same OB are differentially regulated by the different level of odor inputs.

Fate of new neurons in ΔD mouse OB

Firstly, my observation in ΔD mouse OB showed that higher density of immature GCs (days 7-13 after generation) populated in the D-domain than V-domain. This result was rather unexpected, because previous studies showed that migration of new GCs into the OB was either unchanged or suppressed for the sensory-deprived OB by nostril occlusion (Petreanu & Alvarez-Buylla, 2002; Saghatelyan et al, 2004; Yamaguchi & Mori, 2005). This discrepancy might result from the difference of whether sensory deprivation was local or global in the OB. In the nostril-occluded OB, expression of tenascin-R, an extracellular matrix protein, is reduced (Saghatelyan et al, 2004). The

reduced expression of tenascin-R results in the suppressed migration of immature GCs in the OB. It is intriguing to examine tenascin-R expression in the ΔD mouse OB in which strength of olfactory inputs is different between D- and V-domains in a same OB. Alternatively, determination of the direction of radial migration of new GCs in the OB might be controlled by olfactory sensory inputs. Initially, new GCs migrate tangentially along RMS to the core region of the OB. Then they start radial migration from the core region to the GCL of the OB. New GCs may chose the direction of radial migration according to the olfactory sensory input, such that they preferentially chose less activated OB domains. This kind of regulation may become apparent only by local manipulation of OB activity as in ΔD mice. Further examination of ΔD mouse OB would reveal the neuronal mechanisms of how olfactory sensory inputs regulate the recruitment of new GCs in the local OB domain.

Second point of my observation is that survival of new GCs was much reduced in the D-domain compared to V-domain. This result indicated that survival and death of new GCs are controlled in the local OB domain according to the local olfactory inputs. New GCs in the D-domain were drastically eliminated between days 9 and 32 after

generation, the period corresponding to the critical period of sensory experience-dependent survival and death decision of new GCs (Yamaguchi and Mori, 2005). The OB is considered to consist of columnar structures associated with glomerular modules. Olfactory inputs from the OSNs expressing a given type of odorant receptor converge onto a few glomeruli in the OB (Mombaerts, 2004). Following odor stimulation, activated mitral/tufted cells and activated GCs roughly distribute in radial columnar areas corresponding to the activated glomeruli (Xu et al, 2000). Thus survival and death of new GCs might depend on which glomerular modules they belong to and whether or not the glomerular modules are activated by odor stimulation. Through this local control of survival and death of new GCs, new GCs may be incorporated into particular glomerular modules depending on the experienced odor inputs and modulate the activity of mitral/tufted cells within and across the particular glomerular modules.

Behavioral state-dependent life and death decision of new GCs

I showed that survival and death decision of new GCs is linked to wake-sleep behaviors

of the animals. In food-restricted ΔD mice, elimination of new GCs was promoted during postprandial period, especially in association with postprandial behaviors such as resting and sleeping. Further, GC elimination during postprandial period was much prominent in the D-domain compared to the V-domain, indicating that the extent of GC elimination during postprandial period is dependent on prior olfactory sensory inputs.

Given these observations I have proposed a "two-stage model" for the sensory experience-dependent selection of new GCs, in which the two stages represent olfactory sensory experience during food search and eating followed by postprandial behaviors including sleep (Figure 8) (Yokoyama et al. 2011; Yamaguchi et al. 2013). During the waking period, when mice show food-searching and eating behaviors, a subset of newly generated adult-born GCs receives olfactory sensory inputs from mitral/tufted cells via dendrodendritic synapses in the EPL, while the remaining subset does not. I assume that new GCs that are activated by these olfactory sensory inputs receive a kind of synaptic tagging that works as a substrate for subsequent plastic change (Frey and Morris 1997; Redondo and Morris 2011). These GCs may be "tagged" in the dendrodendritic synapses or the cells themselves, while other GCs that are not activated by olfactory

sensory input remain “non-tagged”. Importantly, although differential tagging of new GCs might occur during feeding behavior, the survival and death decision of GCs is not made during feeding. During the subsequent postprandial period, the cell selection process is triggered and the increased GC apoptosis occurs. Yamaguchi and others who are my laboratory members hypothesized that some sort of “reorganizing signal” enters the OB during the postprandial period, typically during the postprandial sleep period, and promotes GC selection according to the presence or absence of tags that the GCs received during the preceding waking period (Yamaguchi et al., 2013). The fate of individual adult-born GCs might be determined by the interplay between tagging that reflect the olfactory sensory experience during the waking period and the hypothetical reorganizing signal that enters the OB during the subsequent period.

This idea of a two-stage model of GC elimination is analogous to the two-stage model of memory formation and consolidation in the hippocampus. This model states that experience-dependent input induces memory trace formation during awake learning and that replay of the experience occurs for the reorganization and consolidation of neuronal circuits during subsequent sleep or rest (Buzsaki 1989; Diekelmann and Born 2010).

Enhanced GC elimination during the postprandial period also resembles homeostatic synaptic downscaling during sleep (Tononi and Cirelli 2006; Vyazovskiy et al. 2008). It has been shown in the rodent neocortex and hippocampus that behavioral state modulates synaptic strength, with a net increase during waking and a reduction during sleep. Because a large number of adult-born GCs are recruited in the OB every day, elimination of adult-born GCs is necessary to maintaining the overall number of GCs in the entire OB within an appropriate range. This kind of downscaling may increase the ratio of useful versus useless GCs, and thereby improve the signal-to-noise ratio for olfactory information processing, as has been proposed for the role of synaptic downscaling (Tononi and Cirelli, 2006), and may make room for a successive cohort of new GCs to be integrated in preparation for the next round of new olfactory experience.

Possible neuronal mechanisms underlying sensory experience- and behavioral state-dependent GC selection

What are the neuronal mechanisms for the hypothetical reorganizing signal during postprandial period? One possibility is that the signal is contributed to by glutamatergic

top-down inputs from the olfactory cortex. Manabe et al. in our laboratory recorded single unit activities in the anterior piriform cortex (APC) in freely-behaving rats, and showed that numerous APC neurons fire synchronously during the slow-wave sleep state (Manabe et al. 2011). Importantly, the synchronous firing of APC neurons during the slow-wave sleep state drives synchronized top-down synaptic inputs to the OB (Manabe et al. 2011). Given that many of the top-down axonal connections from the APC terminate onto GCs in the OB (Luskin and Price, 1983), the synchronized top-down inputs are a plausible candidate for the behavioral state-dependent reorganizing signal for new GCs. Actually, Komano-Inoue et al. in our laboratory have observed that pharmacological suppression of the synchronized top-down inputs during the postprandial period inhibits the increased GC apoptosis (unpublished observation), in favor of the notion that the major contributor to the hypothetical reorganizing signal that promotes GC elimination during the postprandial period is the synchronized top-down input from the olfactory cortex to the OB.

Glutamatargic synaptic inputs often induce neuronal death (Hardingham and Bading, 2010). Summated EPSPs in individual GCs by synchronized glutamatergic top-down

inputs from the OC neurons might induce excitotoxic mechanisms such as the calcium-dependent cell death machinery via the calcium-permeable ionotropic NMDARs (Lai et al., 2013). In addition, T-type calcium channels are highly expressed in GCs (Egger et al., 2003). During slow-wave sleep, membrane potential of GCs might fluctuate between hyperpolarization and depolarization. During the hyperpolarization phase, T-type calcium channels on GCs might recover from inactivation, and then they might be efficiently activated by top-down synaptic inputs during the following depolarization phase. The T-type calcium channel-mediated calcium signal might effectively propagate to the entire GCs and also modulate gene expression in the GCs. I hypothesize that coordinated activity of NMDARs and T-type calcium channels on new GCs plays crucial role in triggering apoptotic GCs death.

I showed that olfactory sensory inputs-induced GCs activity was reduced in the D-domain of ΔD mouse OB (Figure 3). On the other hand, it is totally unknown at present whether the synchronized top-down inputs from the olfactory cortex to the OB occur ubiquitously in the entire OB or occur differently in different OB domains. It is intriguing to examine whether the top-down synaptic inputs during postprandial period

show difference between D- and V-domain of ΔD mouse OB. A possibility is that reduced olfactory sensory inputs to D-domain of ΔD mouse OB in turn modify the occurrence of top-down synaptic inputs to the D-domain. In the hippocampus, synchronized neuronal activity during sleep is known to reflect the neuronal activity during preceding waking period (Wilson and McNaughton, 1994). Considering the possibility that top-down inputs during postprandial period to the OB may also reflect preceding olfactory sensory inputs-mediated activity, analysis of top-down inputs in the D- and V-domain of ΔD mouse OB may provide an important clue to the understanding of the generation mechanisms of synchronized top-down inputs.

Development of dendritic arbors of new GCs in the sensory-input intact and sensory input-deprived OB

In neocortex and hippocampus, interneuron subtypes that make synapses on perisomatic regions of pyramidal cells have been extensively studied (Markram et al., 2004; Somogyi and Klausberger, 2005). However, in the OB, most analyses have been conducted on dendritic-targeting synapses of GCs to the lateral dendrites of

mitral/tufted cells in the EPL. Perisomatic-targeting synapses of GCs to the somata of mitral/tufted cells in the MCL have been paid little attention except for a limited number of analyses including ours (Toida et al, 1994; Naritsuka et al, 2009). I here observed the development of dendritic arbors and protrusions of new GCs both in the EPL and MCL, and found sensory input-dependent regulation of dendritic development in these layers.

In the sensory-intact OB, new GCs extensively developed dendrites and synaptic structures in the EPL. In contrast, in the sensory-deprived OB, new GCs showed poor development of dendrites and synaptic structures in the EPL. Instead, they made many branches and protrusions in the MCL, suggesting that contact formation of sensory-deprived new GCs to mitral cells was biased from the dendrites to the somata of mitral cells.

This alteration might be an adaptation mechanism of new GCs. In the sensory-deprived OB, firing activity of mitral/tufted cells remarkably reduces (Philpot et al, 1997). For new GCs to better survive in the sensory-deprived OB, they might need to effectively receive excitatory synaptic inputs from mitral/tufted cells showing reduced activity. Although depolarizing potential after mitral/tufted cell firing can

back-propagate from the somata to the entire length of lateral dendrites, the depolarizing potential might be attenuated in the distal portion of lateral dendrites, especially by inhibitory synaptic inputs from GCs to the mitral cell lateral dendrites (Xiong and Chen 2002). Thus, it is likely that GCs that make synapses near the somata of mitral cells have much more opportunity of receiving mitral cell-mediated excitatory activity than GCs that make synapses at the distal portion of the lateral dendrites of mitral cells. New GCs in the sensory-deprived OB might try to survive by making synapses preferentially to the somata of mitral cells. Further examination of the dendritic protrusions in the MCL and EPL of new GCs in the sensory-intact and -deprived OB would reveal how new GCs are utilized in the OB neuronal circuit depending on olfactory sensory inputs during waking olfactory behavior and neuronal activities during subsequent rest/sleep behavior.

Acknowledgments

I thank Dr. K. Kobayakawa, Dr. R. Kobayakawa (Department of Functional Neuroscience, Osaka Bioscience Institute) and Prof. H. Sakano (Department of Boiphysics and Biochemistry, Graduate School of Science, the University of Tokyo) for kindly provided of ΔD mouse; Dr. Y. Ohashi and Prof. Y. Miyashita (Department of Physiology, Graduate School of Medicine, the University of Tokyo) for technical advices of lentivirus generation and injection methods.

And I am sincerely grateful to Prof. K. Mori for his general support, supervision and always stimulating us with an interesting idea. The success of this study owes to Dr. M. Yamaguchi for his critical advice and abundant technical support from the beginning of this study. Finally, I would like to show the deepest gratitude for all the members of the Department of Physiology of the University of Tokyo for their valuable discussion all the time.

References

Brown, J.P., Couillard-Despres, S., Cooper-Kuhn, C.M., Winkler, J., Aigner, L., Kuhn, H.G. (2003). Transient expression of doublecortin during adult neurogenesis. J. Comp. Neurol. 467, 1-10.

Buzsaki, G. (1989). Two-stage model of memory trace formation: a role for "noisy" brain states. Neuroscience 31, 551-570.

Carleton, A., Petreanu, L.T., Lansford, R., Alvarez-Buylla, A., Lledo, P.M. (2003). Becoming a new neuron in the adult olfactory bulb. Nat. Neurosci. 6, 507-518.

Diekelmann, S., Born, J. (2010). The memory function of sleep. Nat. Rev. Neurosci. 11, 114-126.

Doty, RL. (1986). Odor-guided behavior in mammals. Experientia 42, 257-271.

Egger, V., Svoboda, K., Mainen, F.Z., (2003). Mechanisms of Lateral Inhibition in the Olfactory Bulb: Efficiency and Modulation of Spike-Evoked Calcium Influx into Granule cells. J. Neurosci. 23(20), 7551-7558.

Fiske, B.K., Brunjes, P.C. (2001). Cell death in the developing and sensory-deprived rat olfactory bulb. J. Comp. Neurol. 431, 311-319.

Frey, U., Morris, R.G.M. (1997). Synaptic tagging and long-term potentiation. Nature 385, 533-536.

Gooley, J.J., Schomer, A., Saper, C.B. (2006). The dorsomedial hypothalamic nucleus is critical for the expression of food-entrainable circadian rhythms. Nat. Neurosci. 9, 398-407.

Hanawa, H., Hematti, P., Keyvanfar, K., Metzger, M.E., Krouse, A., Donahue, R.E., Kepes, S., Gray, J., Dunbar, C.E., Persons, D.A., Nienhuis, A.W. (2004). Efficient gene

transfer into rhesus repopulating hematopoietic stem cells using a simian immunodeficiency virus-based lentiviral vector system. Blood 103, 4062–4069.

Hardingham, G.E., Bading, H. (2010). Synaptic versus extrasynaptic NMDA receptor signalling: implications for neurodegenerative disorders. Nat. Rev. Neurosci. 11(10):682-696.

Kelsch, W., Lin, C.W., Lois, C. (2008). Sequential development of synapses in dendritic domains during adult neurogenesis. Proc. Natl. Acad. Sci. USA. 105, 16803-16808.

Kelsch, W., C.W., Lin, Mosley, C.P., Lois, C. (2009). A Critical Period for Activity-Dependent Synaptic Development during Olfactory Bulb Adult Neurogenesis. Journal of Neuroscience 29(38): 11852-11858.

Kobayakawa, K., Kobayakawa, R., Matsumoto, H., Oka, Y., Imai, T., Ikawa, M., Okabe, M., Ikeda, T., Itohara, S., Kikusui, T., Mori, K., Sakano, H. (2007). Innate versus

learned odour processing in the mouse olfactory bulb. Nature 450, 503-508.

Lai, T.W., Zhang, S., Wang, T.Y., (2013). Excitotoxicity and stroke: Identifying novel targets for neuroprotection. Progress in Neurobiology. (in press)

Lledo, P.M., Alonso, M., Grubb, M.S. (2006). Adult neurogenesis and functional plasticity in neuronal circuits. Nat. Rev. Neurosci. 7, 179-193.

Lois, C., Alvarez-Buylla, A. (1994). Long-distance neuronal migration in the adult mammalian brain. Science 264, 1145-1148.

Luskin, M. B., and Price, J. L. (1983). The topographic organization of associational fibers of the olfactory system in the rat, including centrifugal fibers to the olfactory bulb. J. Comp. Neurol. 216, 264–291.

Luskin, M.B. (1993). Restricted proliferation and migration of postnatally generated neurons derived from the forebrain subventricular zone. Neuron 11, 173-189.

Magavi, S.S.P., Mitchell, B.D., Szentirmai, O., Carter, B.S., Macklis, J.D. (2005). Adult-born and preexisting olfactory granule neurons undergo distinct experience-dependent modifications of their olfactory responses in vivo. J. Neurosci. 25, 10729-10739.

Markram H, Toledo-Rodriguez M, Wang Y, Gupta A, Silberberg G, Wu C. (2004). Interneurons of the neocortical inhibitory system. Nat. Rev. Neurosci. 5(10):793-807.

Matsumoto, H., Kobayakawa, K., Kobayakawa, R., Tashiro, T., Mori, K., Sakano, H., Mori, K. (2010). Spatial arrangement of glomerular molecular-feature clusters in the odorant-receptor-class domains of the mouse olfactory bulb. J. Neurophysiol. 103: 3490-3500

Mistlberger, R.E. (1994). Circadian food-anticipatory activity: formal models and physiological mechanisms. Neurosci. Biobehav. Rev. 18, 171-195.

Mistlberger, R.E., Antle, M.C., Webb, I.C., Jones, M., Weinberg, J., Pollock, M.S. (2003). Circadian clock resetting by arousal in Syrian hamsters: the role of stress and activity. Am. J. Physiol. Regul. Integr. Comp. Physiol. 285, R917-925.

Miyoshi, H., Blomer, U., Takahashi, M., Gage, F.H., Verma, I.M. (1998). Development of a self-inactivating lentivirus vector. J. Virol., 72, pp. 8150–8157

Mombaerts P. (2004). Genes and ligands for odorant, vomeronasal and taste receptors. Nat. Rev. Neurosci, 5, 263.

Mori, K. (1987). Membrane and synaptic properties of identified neurons in the olfactory bulb. Prog. Neurobiol. 29, 275-320.

Naritsuka, H., Sakai, K., Hashikawa, T., Mori, K., Yamaguchi, Y. (2009). Perisomatic-targeting granule cells in the mouse olfactory bulb. J. Comp. Neurol.

515:409-426

Petreanu, L., Alvarez-Buylla, A. (2002). Maturation and death of adult-born olfactory bulb granule neurons: role of olfaction. J. Neurosci. 22, 6106-6113.

Philpot BD, Foster TC, Brunjes PC. (1997). Mitral/tufted cell activity is attenuated and becomes uncoupled from respiration following naris closure. J Neurobiol. 33:374-86.

Redondo, R. L., Morris, R. G. (2011). Making memories last: the synaptic tagging and capture hypothesis. *Nat. Rev. Neurosci.* 12, 17-30.

Rochefort, C., Gheusi, G., Vincent, J., Lledo, P.M. (2002). Enriched odor exposure increases the number of newborn neurons in the adult olfactory bulb and improves odor memory. J. Neurosci. 22, 2679-2689.

Saghatelyan, A., Chevigny, A., Schachner, M., Lledo, P.M. (2004). Tenascin-R mediates

activity-dependent recruitment of neuroblasts in the adult mouse forebrain. Nat. Neurosci. **4**, 347-356.

Saghatelyan, A., Roux, P., Migliore, M., Rochefort, C., Desmaisons, D., Charneau, P, Shepherd, G. M., Lledo, P. M. (2005). Activity-dependent adjustments of the inhibitory network in the olfactory bulb following early postnatal deprivation. Neuron 46, 103-116.

Sejnowski, T.J., Destexhe, A. (2000). Why do we sleep? Brain Res. 886, 208-223.

Shipley MT,. Ennis, M. (1996). Functional organization of olfactory system. *J.* Neurobiol. 30, 123-176.

Somogyi P, Klausberger T. (2005). Defined types of cortical interneurone structure space and spike timing in the hippocampus. J Physiol 562(Pt 1):9-26.

Suzuki, A., Obi, K., Urabe, T., Hayakawa, H., Yamada, M., Kaneko, S., Onodera, M., Mizuno, Y., Mochizuki, M. (2002). Feasibility of ex vivo gene therapy for neurological disorders using the new retroviral vector GCDNsap packaged in the vesicular stomatitis virus G protein. J. Neurochem. 82,953–960

Toida, K., Kosaka, K., Heizmann, C.W., Kosaka, T. (1994). Synaptic contacts between mitral/tufted cells and GABAergic neurons containing calcium-binding protein parvalbumin in the rat olfactory bulb, with special reference to reciprocal synapses between them. Brain Res 650(2):347-352.

Tononi, G., Cirelli, G. (2006). Sleep function and synaptic homeostasis. Sleep Med. Rev. 10(1), 49-62.

Vyazovskiy V.V., Cirelli C., Pfister-Genskow M., Faraguna U., Tononi G. (2008). Molecular and electrophysiological evidence for net synaptic potentiation in wake and depression in sleep. Nat. Neurosci. 11(2):200-208.

Whitman, M.C., Greer, C.A. (2007). Synaptic integration of adult-generated olfactory bulb granule cells: basal axodendritic centrifugal input precedes apical dendrodendritic local circuits. J. Neurosci. 27, 9951-9961.

Wilson, M. A., McNaughton, B. L. (1994). Reactivation of hippocampal ensemble memories during sleep. Science 265, 676–679.

Xiong, W., Chen, W.R. (2002). Dynamic gating of spike propagation in the mitral cell lateral dendrites. Neuron 34:115-126

Xu, F., Greer, C.A., Shepherd, G.M. (2000). Odor maps in the olfactory bulb. Journal of Comparative Neurology 422, 489-495.

Yamaguchi, M., Mori, K. (2005). Critical period for sensory experience-dependent

survival of newly generated granule cells in the adult mouse olfactory bulb. Proc. Natl. Acad. Sci. USA. 102, 9697-9702.

Yamaguchi M, Manabe H, Murata K, Mori K. (2013). Reorganization of neuronal circuits of the central olfactory system during postprandial sleep. Front Neural Circuits 7:132

Yokoyama, K.T., Mochimaru, D., Murata, K., Manabe, H., Kobayakawa, K., Kobayakawa, R., Sakano, H., Mori, K., and Yamaguchi, M., (2011). Elimination of Adult-Born Neurons in the Olfactory Bulb Is Promoted during the Postprandial Period. Neuron 71(5): 883-897.

Yoshihara, Y., Kawasaki, M., Tamada, A., Fujita, H., Hayashi, H., Kagamiyama, H., and Mori, K. (1997). OCAM: A new member of the neural cell adhesion molecule family related to zone-to-zone projection of olfactory and vomeronasal axons. J. Neurosci. 17, 5830-5842.

Figure legends

Figure 1. Schematic diagram illustrating the generation, migration and incorporation of adult-born GCs in the OB

GCs (pink) are generated at SVZ and migrate tangentially to the OB through RMS. About 7 days after generation, adult-born GCs reach the OB and start radial migration in the OB. During days 14-28 after generation, GCs extensively make synapses in the OB, and olfactory sensory experience-dependent survival and death decision of GCs significantly occurs during this period. In this critical period for survival and death decision, half of new GCs incorporate into the OB circuitry, and reminder are eliminated from the OB circuitry.

Figure 2. Olfactory sensory inputs lack in the D-domain of the ΔD mouse OB.

(A) In the dorsal domain (D-domain) of ΔD mouse OB, glomeruli are lacking due to the specific depletion of OSNs in the dorsal zone of olfactory epithelium whose axons are to be targeted to the D-domain of the OB. Thus, the ΔD mouse OB has the olfactory sensory inputs-deleted D-domain and the olfactory sensory inputs-intact ventral domain (V-domain). GCs in the D-domain of ΔD mouse OB are presumed not to receive olfactory sensory inputs which are transferred from OSNs to GCs via mitral/tufted cells in the OB. **(**B**)** D- and V-domains of ΔD mouse and wild-type mouse OB shown by anti-OCAM antibody (red) and DAPI (blue) staining. White lines indicate the boundary between the D- and V-domain. In ΔD mouse OB (left), glomeruli are lacking in the D-domain and the remaining glomeruli in the V-domain are OCAM-positive (arrow). In wild-type mouse OB (right), OCAM-negative (arrowhead) and -positive (arrow) glomeruli are clustered in the D- and V-domains, respectively. Thin white lines indicate the boundary between granule cell layer (GCL) and core. IPL, internal plexiform layer; MCL, mitral cell layer; EPL, external plexiform layer; GL, glomerular layer; ONL, olfactory nerve layer. D, dorsal; V, ventral; M, medial; L, lateral. Scale: 200 μm. **(**C**)** Unrolled glomerular maps. Glomerular distribution in OB coronal sections was aligned by centering the dorsal portion. In ΔD mouse OB (left), areas without glomeruli are shown in light blue. Areas with OCAM-positive glomeruli are shown in red. In wild-type mouse OB (right), areas with OCAM-negative glomeruli are shown in dark blue. Areas with OCAM-positive glomeruli are shown in red. Quantitative analyses in

Figures 4-7 were performed using coronal sections covering the central portion of the OB (black asterisks and boxes). Scale: 1 mm.

Figure 3. Odor-induced c-fos activity is reduced in GCs in the D-domain of ΔD mouse OB.

Comparison of c-fos expression in GCs in the D-domain between ΔD and wild-type mouse OB induced by propionic acid stimulation. Blue lines surround D-domain GCL and red lines surround V-domain GCL. Zonal boundary is indicated by white lines. Boxed areas are magnified and shown in the insets. Scale: 200 μm (low power view) and 50 μm (inset).

Figure 4. Local deprivation of olfactory sensory inputs reduces the survival of adult-born GCs in the local OB domain.

(A) BrdU-labeled cells in ΔD and wild-type mouse OB. Labeled cells of ΔD mouse (upper row) and wild-type mouse (lower row) OBs at days 9-13 (left) and days 56-60 (right) after labeling are shown. Blue lines surround D-domain GCL and red lines surround V-domain GCL. Boundary between the D- and V-domain is indicated by white lines. Scale: 200 μm. Note that larger density of labeled cells was observed in the D-domain at days 9-13, but not in the D-domain at days 56-60, in ΔD mouse OB. (B-E) Decreased survival of new GCs in the D-domain of ΔD mouse OB. BrdU was injected for 5 days and labeled GCs were analyzed at the indicated periods. Labeled GC density in the D- and V-domain of ΔD mouse OBs (B), wild-type mouse OBs (C), and ratio of labeled GC density between domains (D-domain/V-domain) of ΔD and wild-type mouse OBs (D) are shown. Survival rates of BrdU-labeled GCs (labeled cell number at days 56-60 / labeled cell number at days 9-13) in the D- and V-domains of ΔD and wild-type mouse OBs are indicated (E). (F) Number of BrdU-positive cells at days 9-13 after BrdU injection in the whole OB of WT and ΔD mouse. **$p<0.01$; ***$p<0.001$; one-way ANOVA with post hoc Bonferroni test (B, C, D, and E) and unpaired t test (F).

Figure 5. Local sensory deprivation enhances GC apoptosis in the local OB domain during feeding and postprandial period.

(A) Restricted feeding protocol. On days 1-10, food was supplied for only 4 hours (11:00-15:00) per day. On day 10, mice were analyzed at 11:00 and 13:00 (arrows).

Mice were maintained under a 12-hour light-dark cycle (light on, 5:00-17:00, white bars; light off, 17:00-5:00, gray bars). (B) Caspase-3-activated apoptotic GCs in the D- and V-domain of ΔD mouse OB before feeding (11:00, left panels) and after showing feeding and postprandial behaviors (13:00, right panels). Blue lines surround D-domain GCL and red lines surround V-domain GCL. Boundary between the D- and V-domain is indicated by white lines. Boxed areas are magnified and shown. Scale: 200 μm (low power view) and 50 μm (high power view). (C and D) Density of caspase-3-activated GCs in the D- and V-domain of ΔD mouse (C) and wild-type mouse (D) OBs before and 2 hours after the start of food supply. (E) Ratio of the density of caspase-3-activated GCs (D-domain/V-domain) in ΔD and wild-type mouse OBs before and 2 hours after the start of food supply. The ratio between domains is calculated in each OB and the data from different mice are averaged. (F) Density of TUNEL-positive GCs in the D- and V-domains of ΔD mouse OB before and 2 hours after the start of food supply. The density remarkably increased in the D-domain 2 hours after the start of food supply. **$p<0.01$; ***$p<0.001$; n.s., not significant; unpaired t test (C, D, E, and F).

Figure 6. Local sensory input-dependent enhancement of GC apoptosis occurs in association with postprandial behavior.

(A) Behaviors of ΔD mice during the initial 2 hours after the start of food supply under the 10 days-food restriction paradigm. Behaviors are categorized and the frequency of each behavior is shown in the histograms. Data represent the frequency averaged from 6 animals. (B and C) Effect of disturbance of postprandial behavior on enhanced GC apoptosis in D-domain (B) and V-domain (C) of ΔD mouse OB. Each group of mice was analyzed at the indicated times with or without postprandial behavior disturbance throughout the period from the food delivery to the analysis time points. ***$p<0.001$; n.s., not significant; one-way ANOVA with post hoc Bonferroni test (B and C).

Figure 7. A majority of apoptotic GCs in the ΔD mouse OB are adult-born GCs.

(A and B) Percentage of caspase-3-activated GCs in the D-domain (A) and V-domain (B) of ΔD mouse OB positive for BrdU, DCX and either BrdU or DCX. BrdU-labeled GCs are 14-20 days of age. Data before and 2 hours after the start of food supply are indicated. More than 50 % of caspase-3-activated GCs are positive for either BrdU or DCX in both domains. n.s., not significant; unpaired t test (A and B).

Figure 8. Schematic diagram of two-stage model for GC elimination in the ΔD mouse OB

Adult-born GCs (green, Gr) make reciprocal synapses with mitral/tufted cells (yellow, M/T) and receive top-down synaptic input from pyramidal cells in the olfactory cortex (gray, Py). (left panels) During waking, local sensory input from olfactory sensory neurons (red, OSNs) activates adult-born GCs in V-domain (lower panel) but not adult-born GCs in D-domain (upper panel). (right panels) During the following postprandial period, a hypothetical reorganizing signal enters the OB. Adult-born GCs in V-domain activated during the waking period survive (lower), while not activated adult-born GCs in D-domain are eliminated (upper). Candidates for the reorganizing signal are glutamatergic input from the olfactory cortex, neuromodulatory input, and hormonal signals.

Figure 9. Local sensory deprivation inhibits the development of dendritic protrusions of adult-born GCs in the EPL of the OB.

Newly generated GCs of ΔD mice were labeled by injecting GFP-expressing retrovirus in the SVZ. After 28 days of retrovirus injection, the mice were fixed. Pictures are maximal projection of GFP labeled GCs in D- and V-domains of the ΔD mouse OB. Boxed areas (red squares) are shown in high power view (right panels). Scale: 20 μm (low power view), 5 μm (high power view).

Figure 10. Schematic diagram of lentiviral vector-mediated GFP labeling of adult-born GCs and experimental procedures for the analysis of dendritic morphology of the GFP-labeled GCs

(A) Newly generated GCs migrating in the RMS were labeled by EGFP-expressing lentivirus. (B) Experimental procedure. (Most upper bar) After 5 days of lentivirus injection food restriction started. A group of mice received unilateral nostril occlusion on the first day of food restriction. Mice were analyzed on day 14 (on day 10 of food restriction). (Lower two bars) Restricted feeding protocol. Food was delivered between 11:00 and 15:00. Mice were analyzed on day 10 of food restriction at 9:00, 11:00, 12: 00 and 13:00 (arrows).

Figure 11. Different dendritic arborization of adult-born GCs in the sensory-intact and sensory-deprived OB

(A) Maximal projection pictures of dendrites in the EPL and MCL of GFP-labeled adult-born GC in the sensory-intact (left) and sensory-deprived (right) mouse OB. Scale bar: 7.5 μm. (B and C) Number of branch points of individual GCs in the EPL (B) and MCL (C) in the sensory-intact and -deprived OB. (D and E) Total length of the EPL dendrite (D) and MCL dendrite (E) of individual GCs in the sensory-intact and -deprived OB. Bars in each graph indicate the average. **$p<0.01$; ***$p<0.001$; unpaired t test (C, D, and E).

Figure 12. Adult-born GCs in the sensory-deprived OB generate large number of dendritic protrusions in the MCL compared to EPL.

(A) Magnified view of maximal projection pictures of MCL dendrites of GFP-labeled adult-born GC in the sensory-intact (left) and -deprived mouse OB. Scale bar: 3 μm. (B and C) Protrusion density in the EPL dendrite (B) and MCL dendrite (C) of adult-born GCs in the sensory-intact and -deprived OB. (D and E) Number of protrusions in the EPL dendrite (D) and MCL dendrite (D) of adult-born GCs in the sensory-intact and -deprived OB. (F) Percentages of protrusions in the MCL among total protrusions (MCL and EPL) of individual adult-born GCs. **$p<0.01$; ***$p<0.001$; n.s., not significant; unpaired t test (C, D, and E)

Figure 13. Ratio of large-headed spines increased among the dendritic protrusions in the MCL of adult-born GCs in the sensory-deprived OB.

(A and C) Distribution of head diameter of protrusions in the EPL (A) and in the MCL (C) of adult-born GCs in the sensory-intact and -deprived OB. (B and D) Cumulative graphs of head diameter of protrusions in the EPL (B) and in the MCL (D) of adult-born GCs in the sensory-intact and -deprived OB. Statistical analysis is conducted by unpaired nonparametric Kolmogorov-smirnov test (A and B: $p=0.1082$, C and D: $p=0.0217$). Number of analyzed protrusions: 593 from 10 cells for EPL protrusions of new GCs in sensory-intact OB, 140 from 10 cells for EPL protrusions of new GCs in sensory-deprived OB, 117 from 10 cells for MCL protrusions of new GCs in sensory-intact OB, and 282 from 10 cells for MCL protrusions of new GCs in sensory-deprived OB.

Figure 1

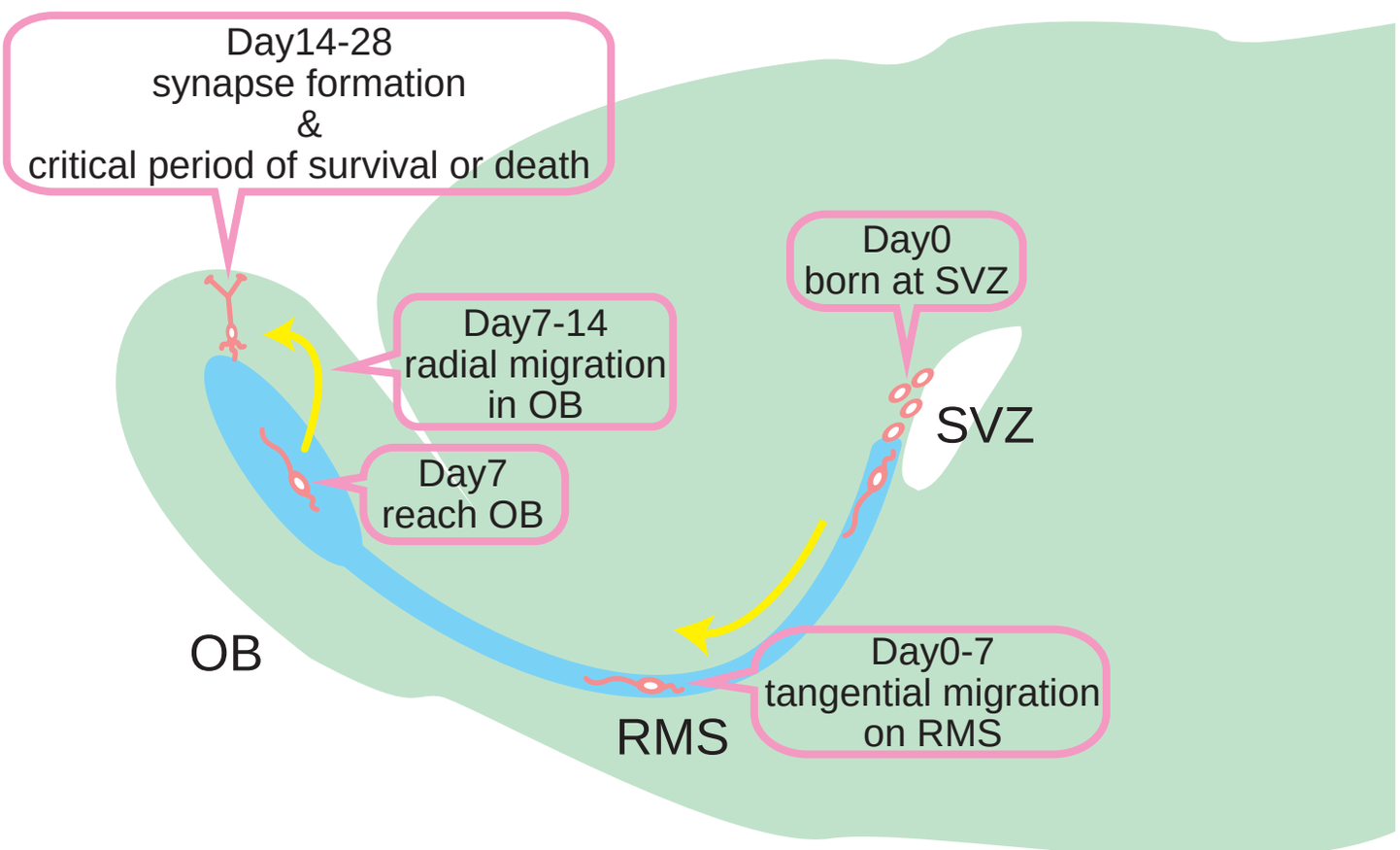
Day14-28
synapse formation
&
critical period of survival or death
Day0
born at SVZ
Day7-14
radial migration
in OB
SVZ
Day7
reach OB
OB
Day0-7
tangential migration
on RMS
RMS

Figure 2

A

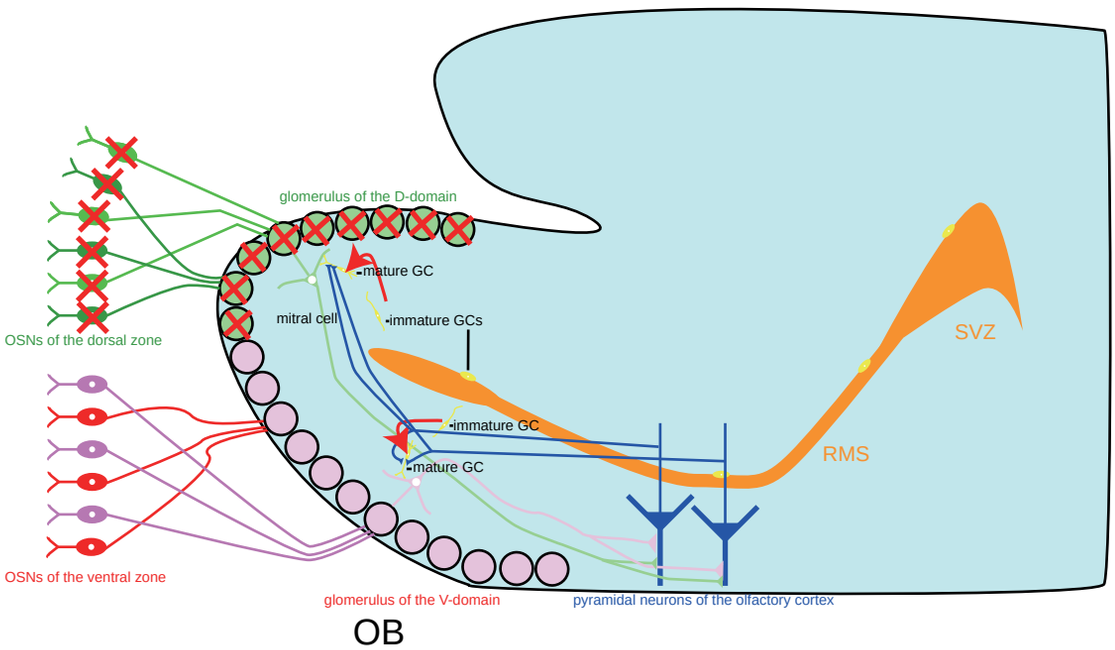
glomerulus of the D-domain
mature GC
mitral cell
immature GCs
OSNs of the dorsal zone
SVZ
immature GC
mature GC
RMS
OSNs of the ventral zone
glomerulus of the V-domain
pyramidal neurons of the olfactory cortex
OB

B

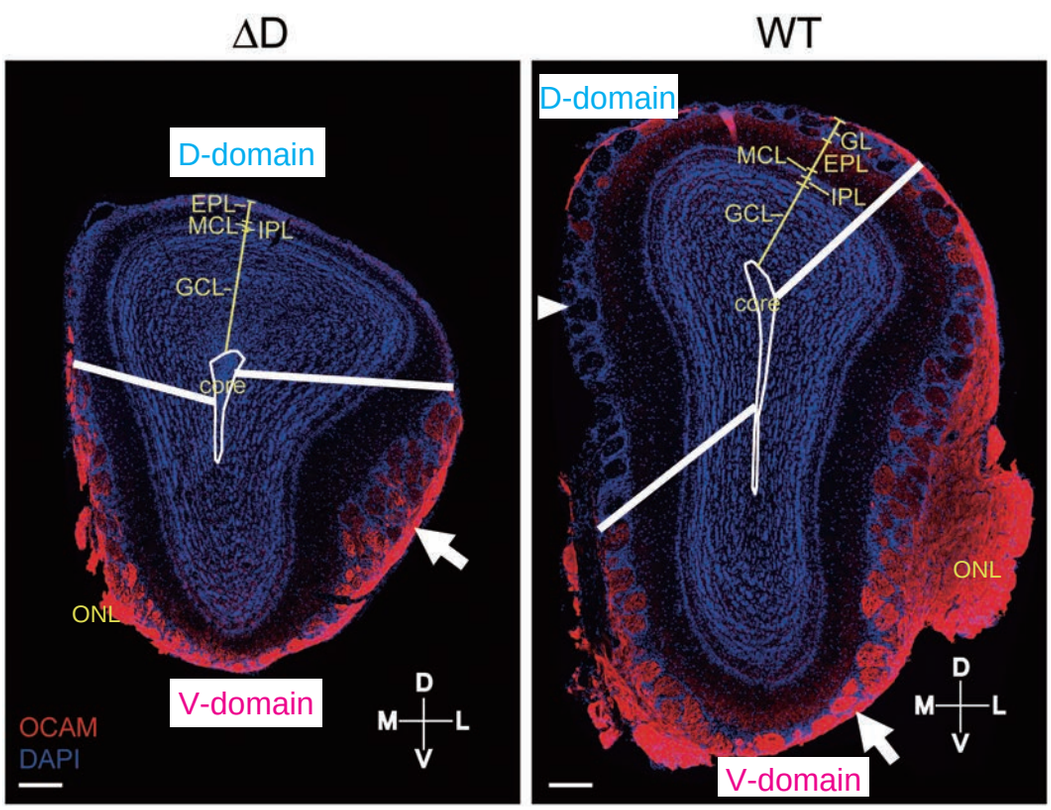
ΔD
WT
D-domain
EPL
MCL
IPL
GCL
core
ONL
V-domain
OCAM
DAPI
D
M
L
V
D-domain
MCL
GL
EPL
IPL
GCL
core
ONL
V-domain
D
M
L
V

C

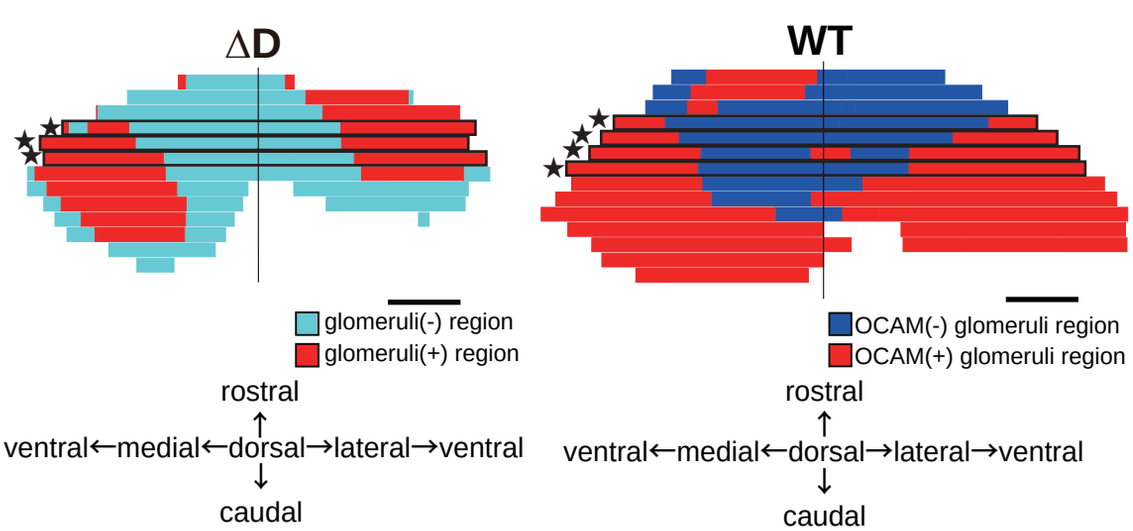
ΔD
WT
glomeruli(-) region
glomeruli(+) region
OCAM(-) glomeruli region
OCAM(+) glomeruli region
rostral
ventral←medial←dorsal→lateral→ventral
caudal
rostral
ventral←medial←dorsal→lateral→ventral
caudal

Figure 3

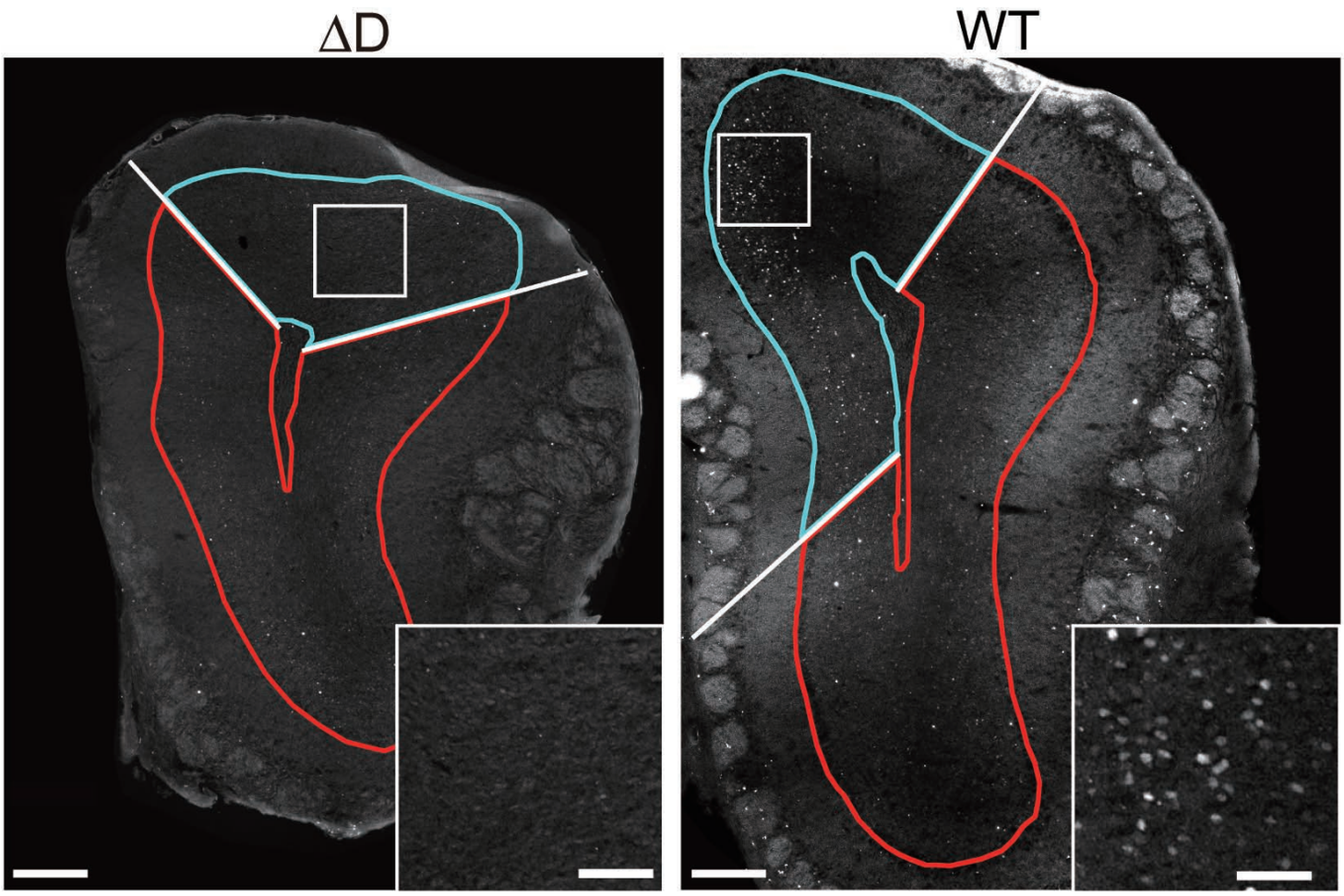

Figure 4

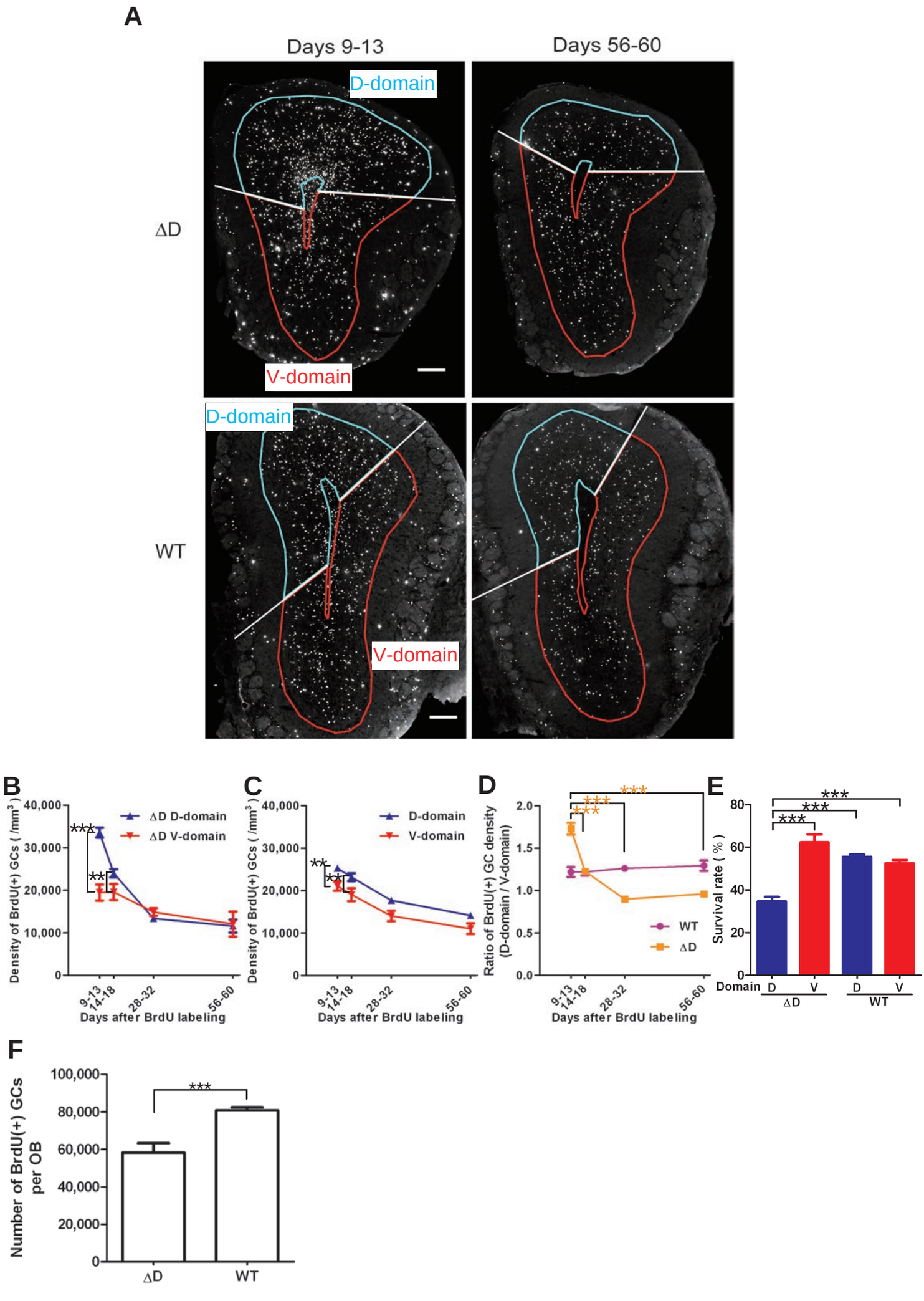
A
Days 9-13
Days 56-60
D-domain
V-domain
ΔD
WT
B
Density of BrdU(+) GCs (/mm³)
ΔD D-domain
ΔD V-domain
Days after BrdU labeling
C
D-domain
V-domain
D
Ratio of BrdU(+) GC density (D-domain / V-domain)
WT
ΔD
E
Survival rate (%)
Domain
F
Number of BrdU(+) GCs per OB

Figure 5

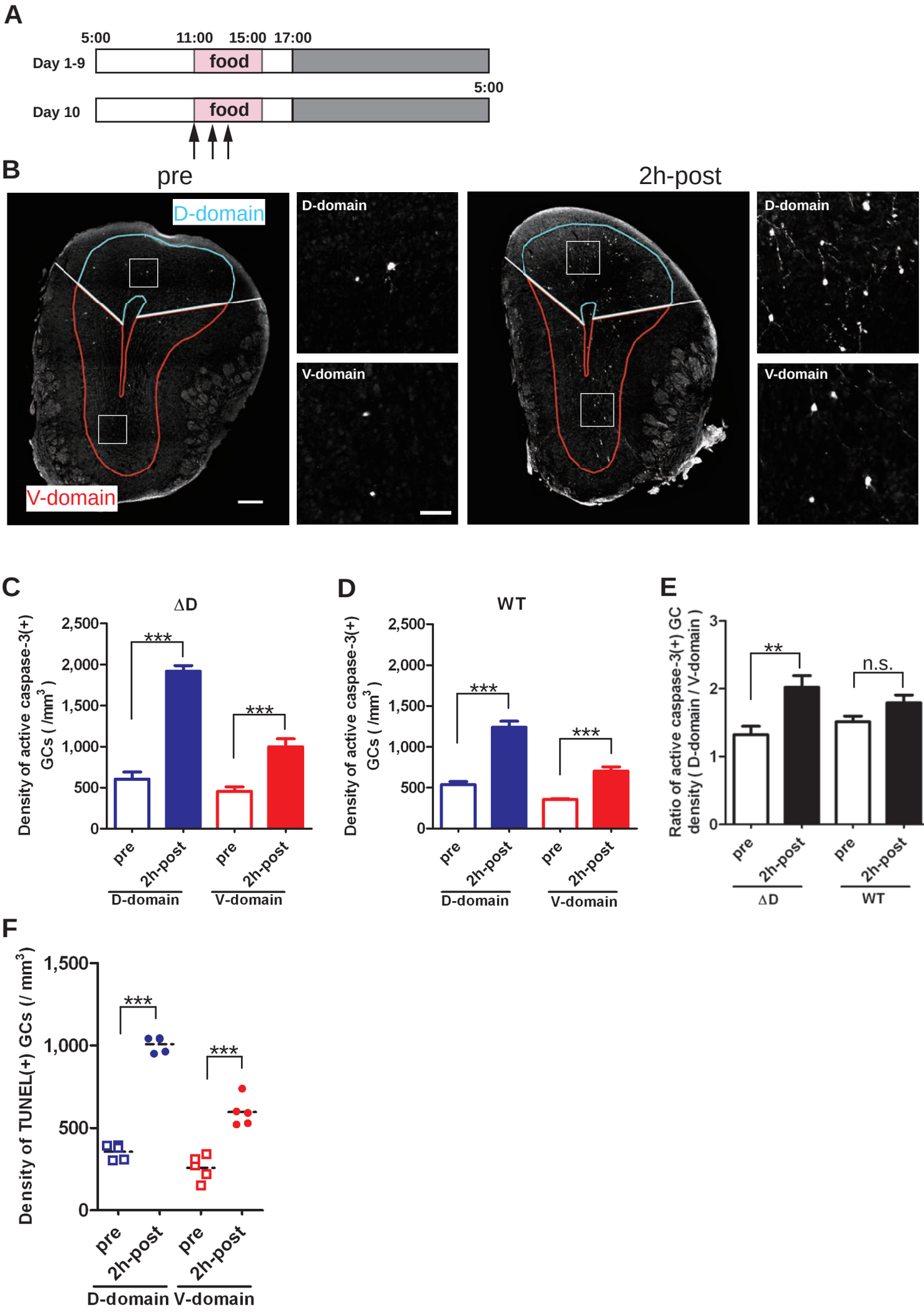
A
5:00
11:00
15:00
17:00
Day 1-9
food
5:00
Day 10
food
B
pre
2h-post
D-domain
V-domain
C
ΔD
Density of active caspase-3(+) GCs (/mm3)
2,500
2,000
1,500
1,000
500
0
***
***
pre
2h-post
pre
2h-post
D-domain
V-domain
D
WT
Density of active caspase-3(+) GCs (/mm3)
***
***
D-domain
V-domain
E
Ratio of active caspase-3(+) GC density (D-domain / V-domain)
3
2
1
0
**
n.s.
ΔD
WT
F
Density of TUNEL(+) GCs (/ mm3)
1,500
1,000
500
0
***
***
D-domain V-domain

Figure 6

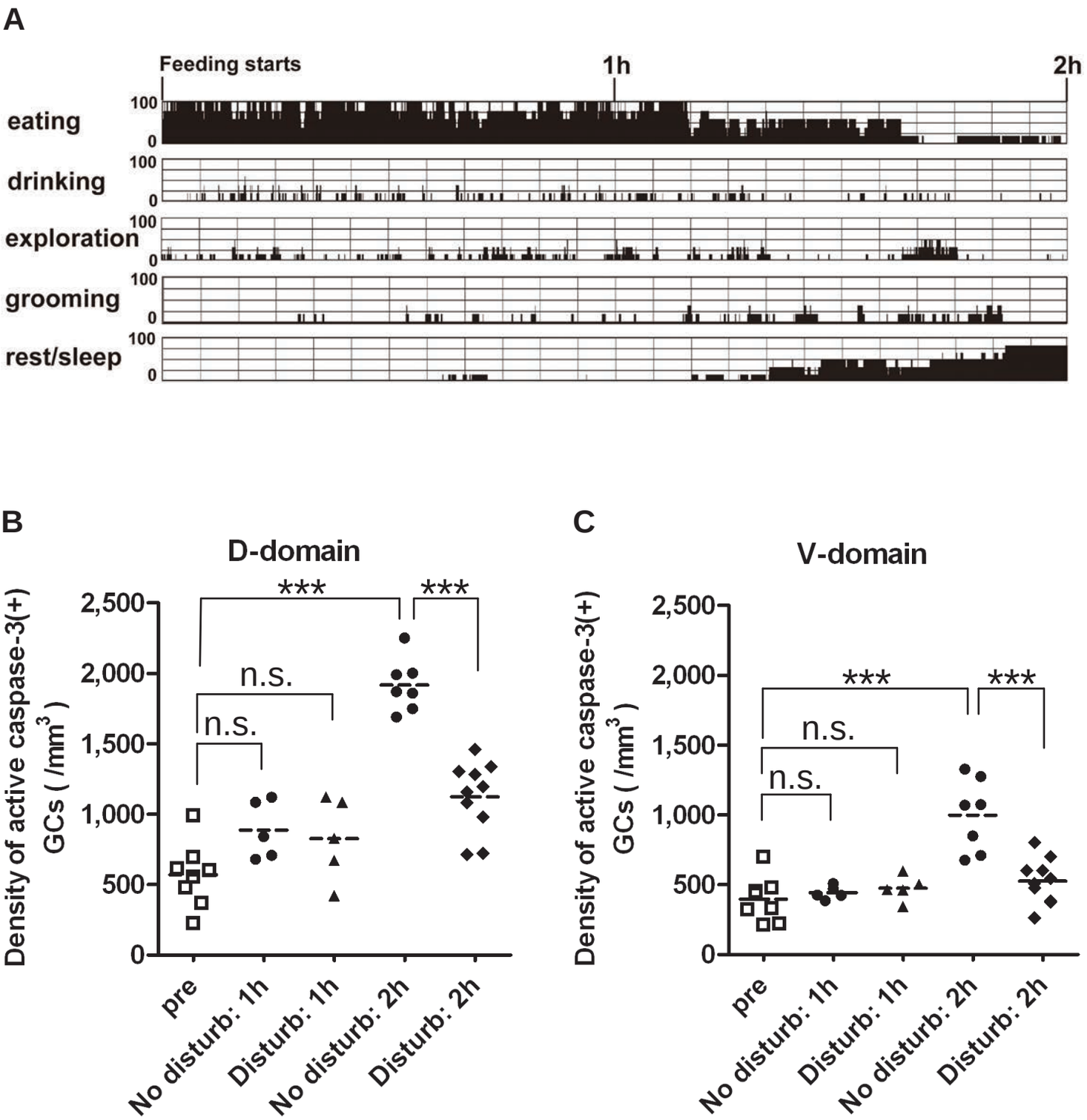
A
Feeding starts
1h
2h
eating
drinking
exploration
grooming
rest/sleep
100
0
B
D-domain
Density of active caspase-3(+) GCs (/mm3)
2,500
2,000
1,500
1,000
500
0
***
***
n.s.
n.s.
pre
No disturb: 1h
Disturb: 1h
No disturb: 2h
Disturb: 2h
C
V-domain
Density of active caspase-3(+) GCs (/mm3)
2,500
2,000
1,500
1,000
500
0
***
***
n.s.
n.s.
pre
No disturb: 1h
Disturb: 1h
No disturb: 2h
Disturb: 2h

Figure 7

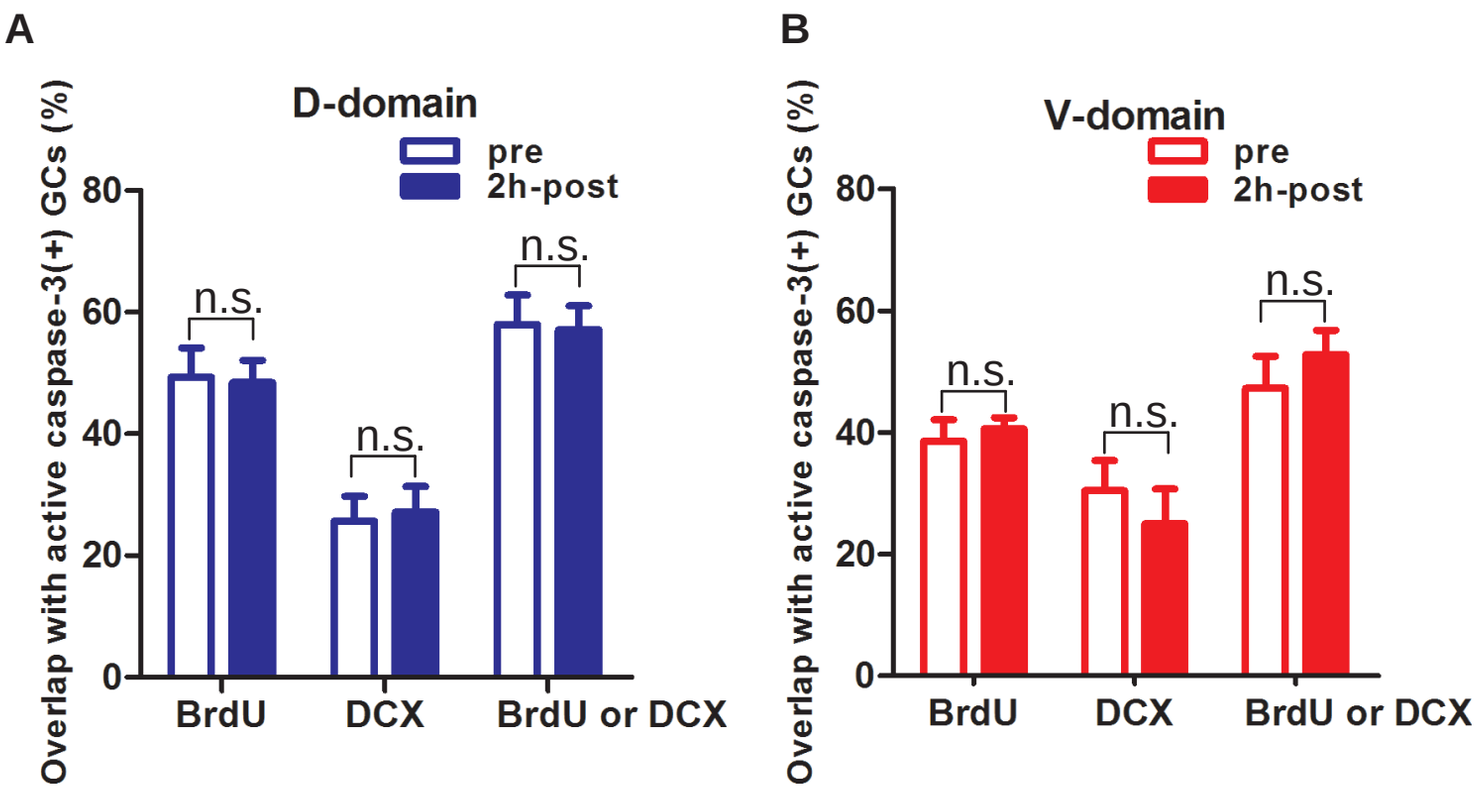
A
D-domain
pre
2h-post
Overlap with active caspase-3(+) GCs (%)
80
60
40
20
0
n.s.
n.s.
n.s.
BrdU
DCX
BrdU or DCX
B
V-domain
pre
2h-post
Overlap with active caspase-3(+) GCs (%)
80
60
40
20
0
n.s.
n.s.
n.s.
BrdU
DCX
BrdU or DCX

Figure 8

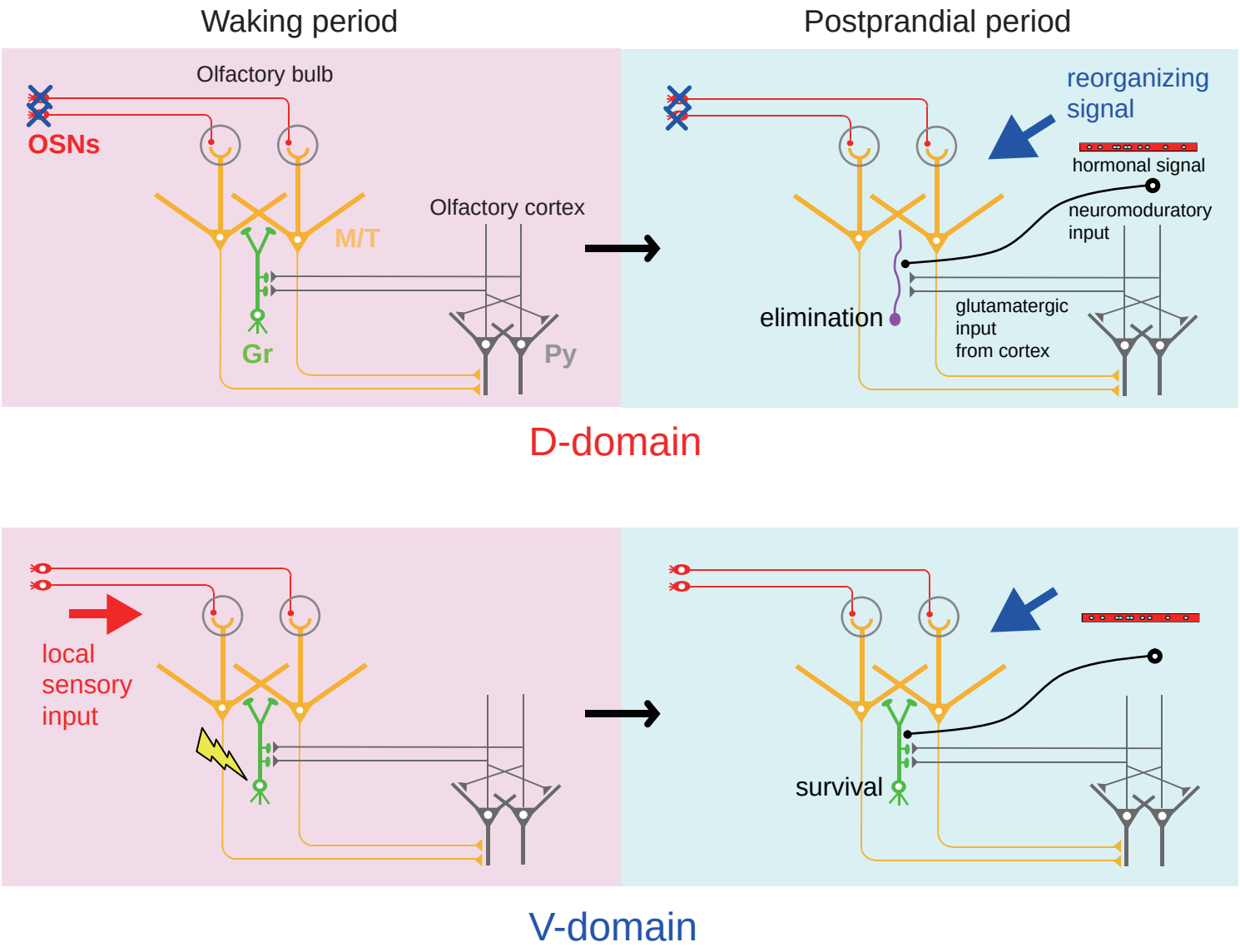
Waking period
Postprandial period
Olfactory bulb
OSNs
M/T
Gr
Olfactory cortex
Py
reorganizing signal
hormonal signal
neuromoduratory input
elimination
glutamatergic input from cortex
D-domain
local sensory input
survival
V-domain

Figure 9

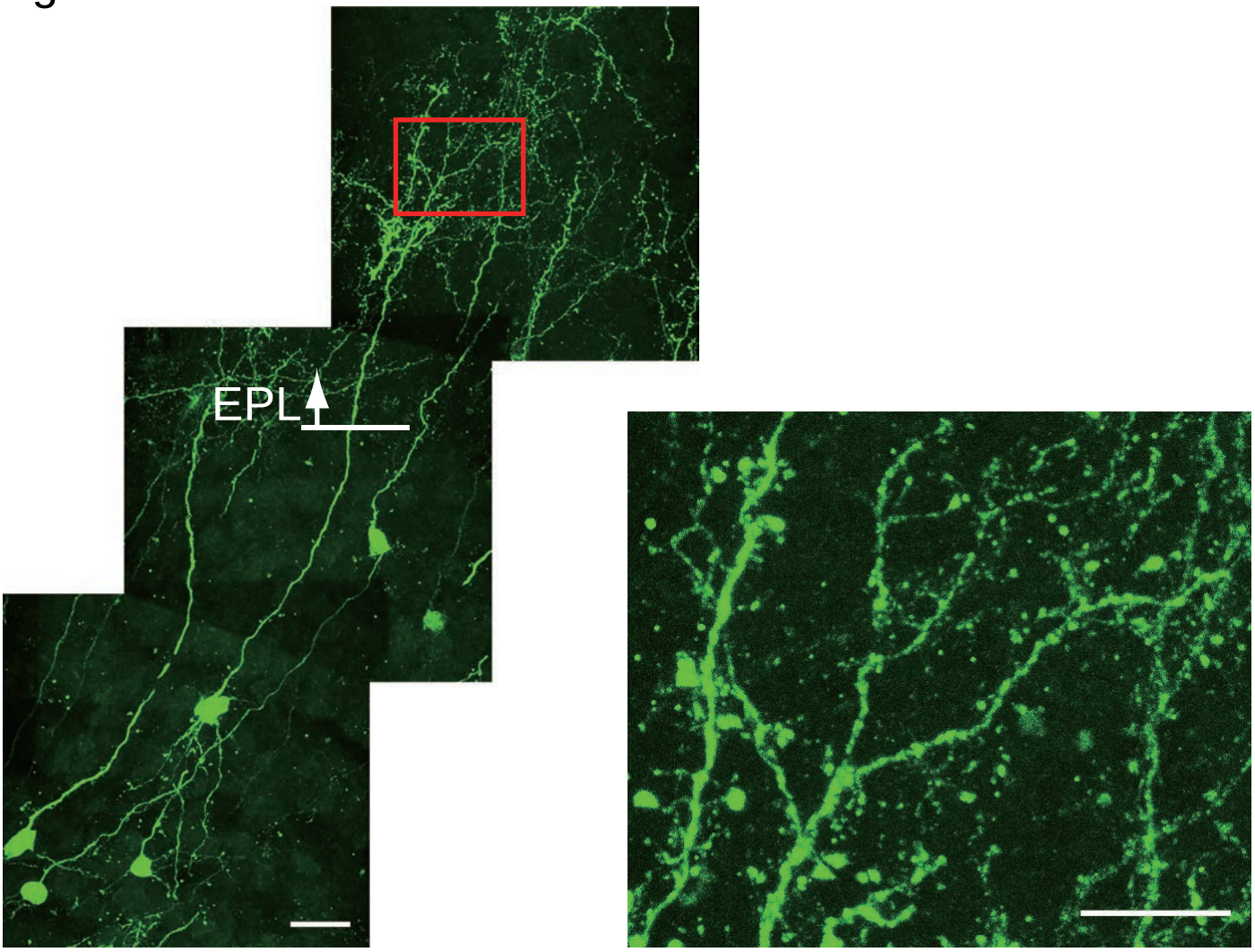

V-domain

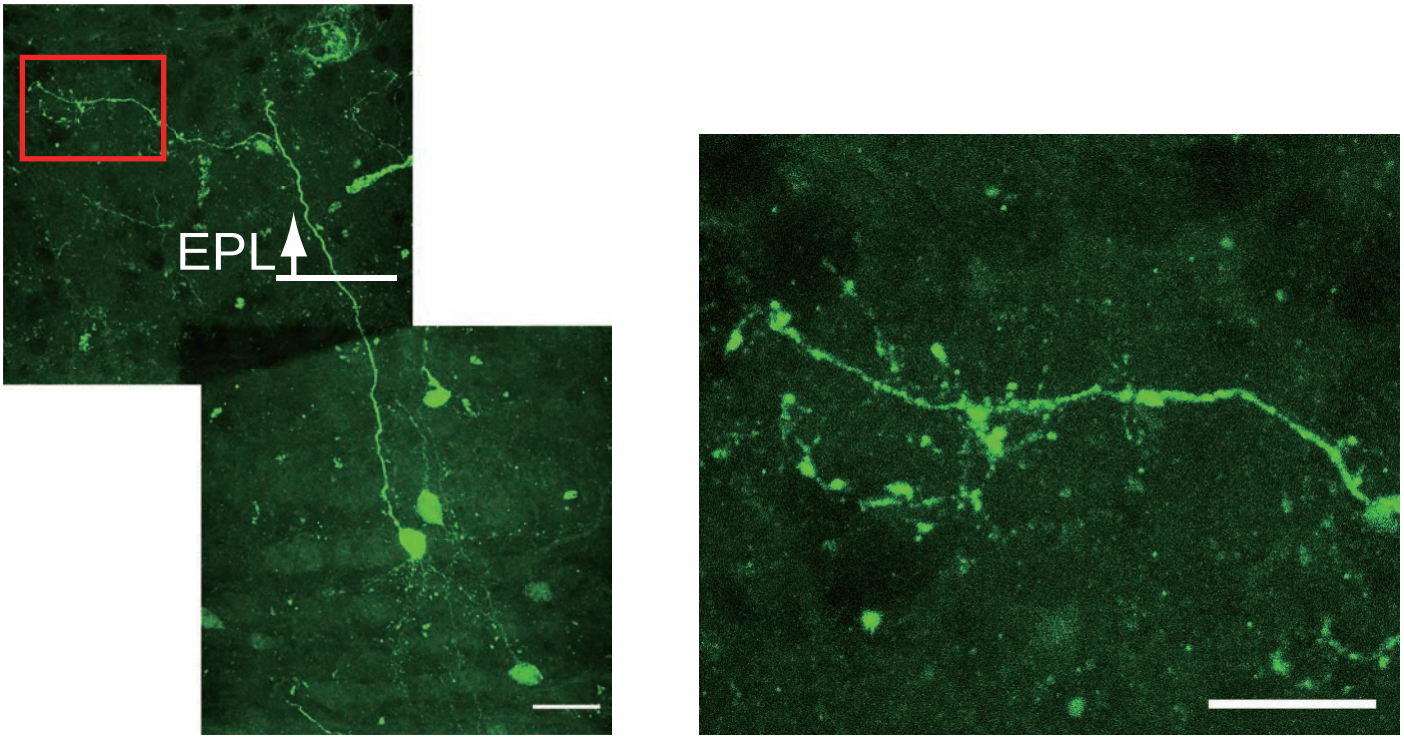

D-domain

Figure 10

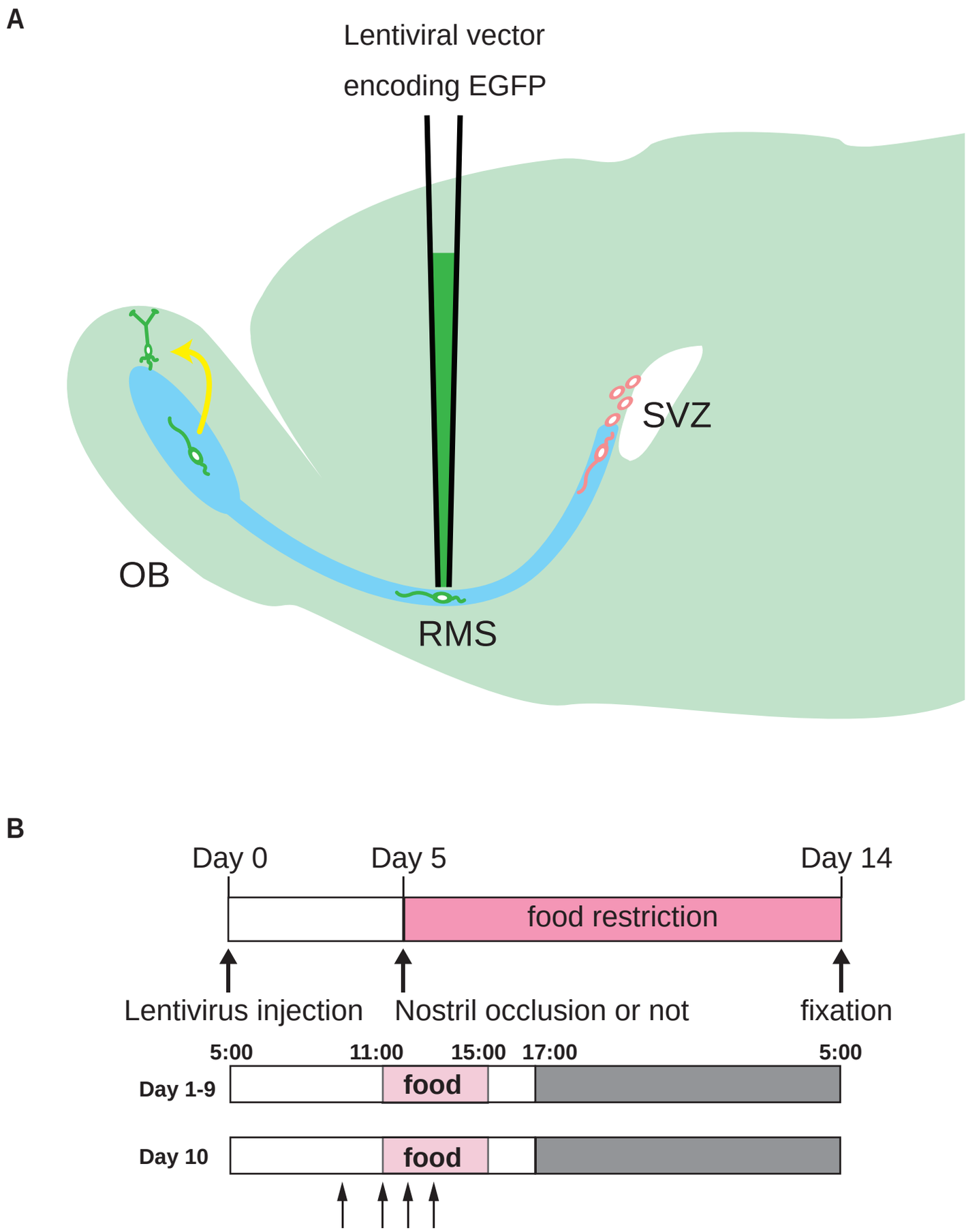
A
Lentiviral vector
encoding EGFP
SVZ
OB
RMS
B
Day 0
Day 5
Day 14
food restriction
Lentivirus injection
Nostril occlusion or not
fixation
5:00
11:00
15:00
17:00
5:00
Day 1-9
food
Day 10
food

Figure 11

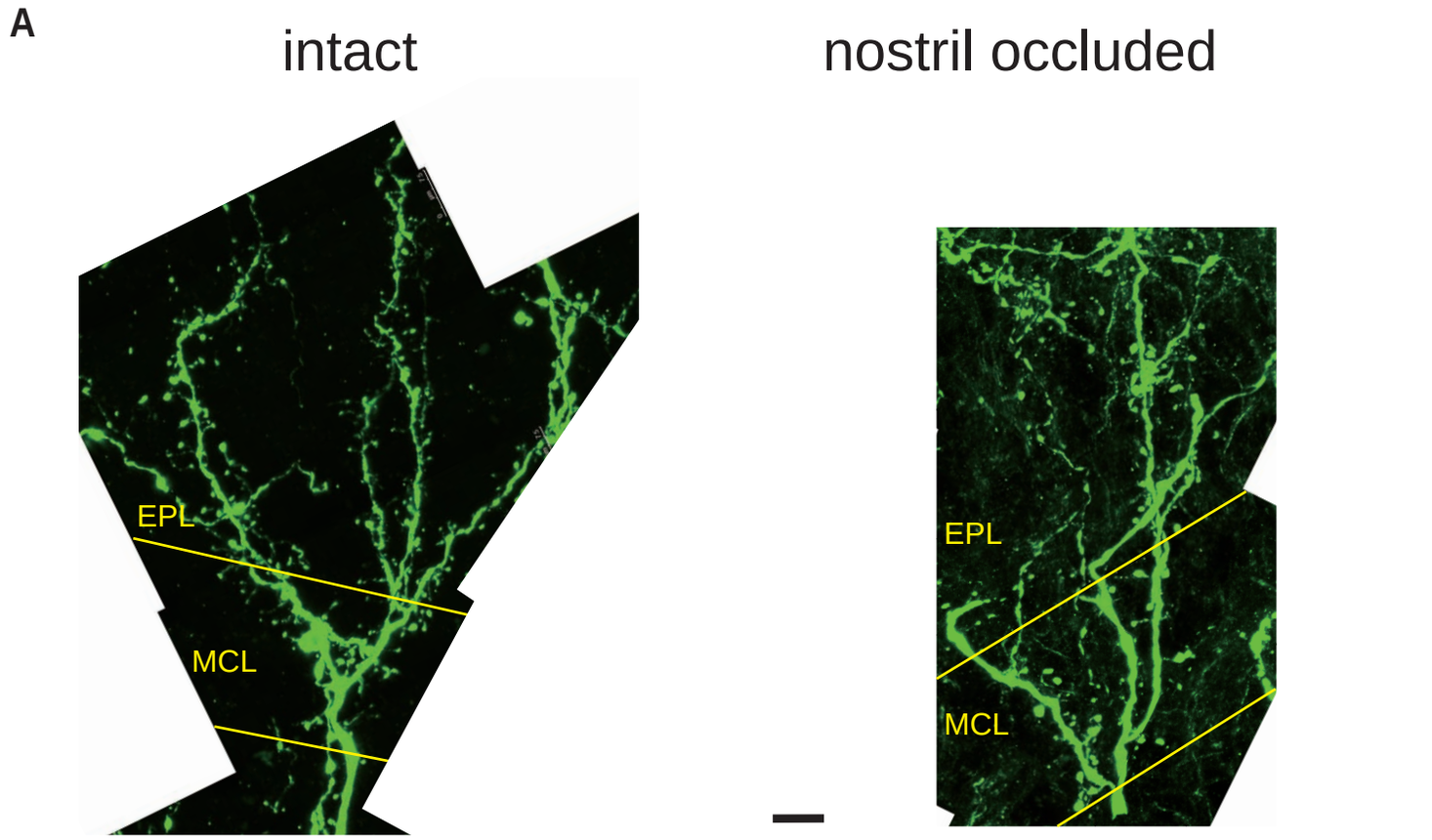
A
intact
nostril occluded
EPL
MCL
EPL
MCL

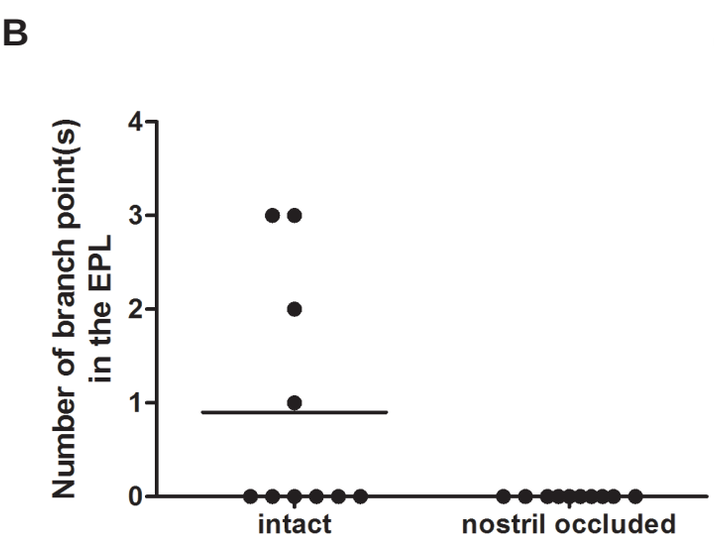
B
Number of branch point(s) in the EPL
0
1
2
3
4
intact
nostril occluded

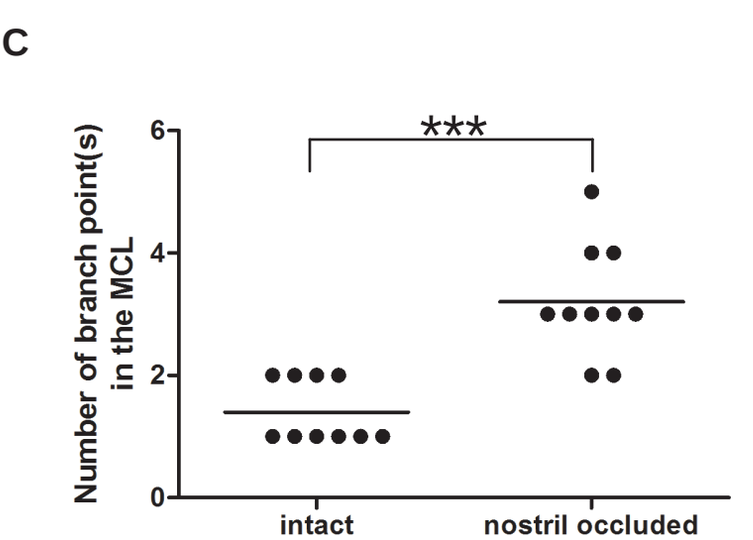
C
Number of branch point(s) in the MCL
0
2
4
6
***
intact
nostril occluded

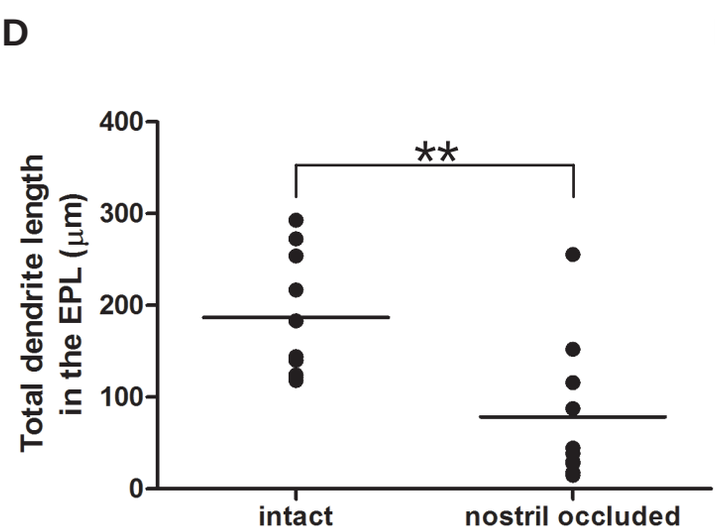
D
Total dendrite length in the EPL (μm)
0
100
200
300
400
**
intact
nostril occluded

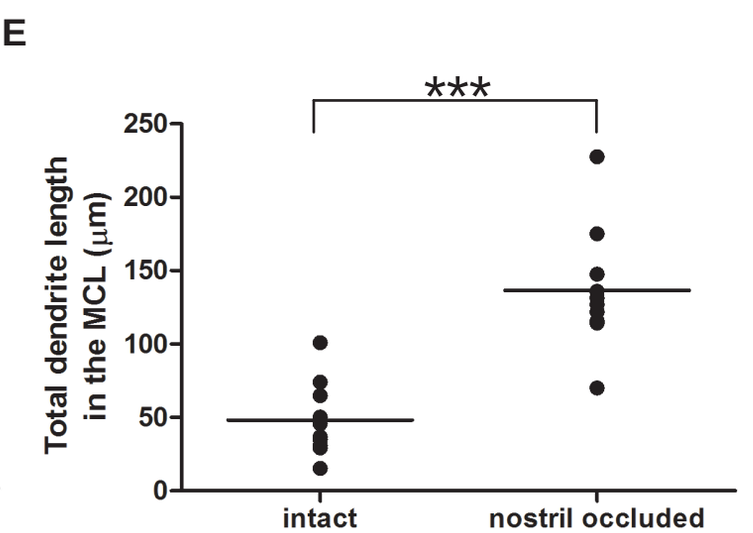
E
Total dendrite length in the MCL (μm)
0
50
100
150
200
250
***
intact
nostril occluded

Figure 12

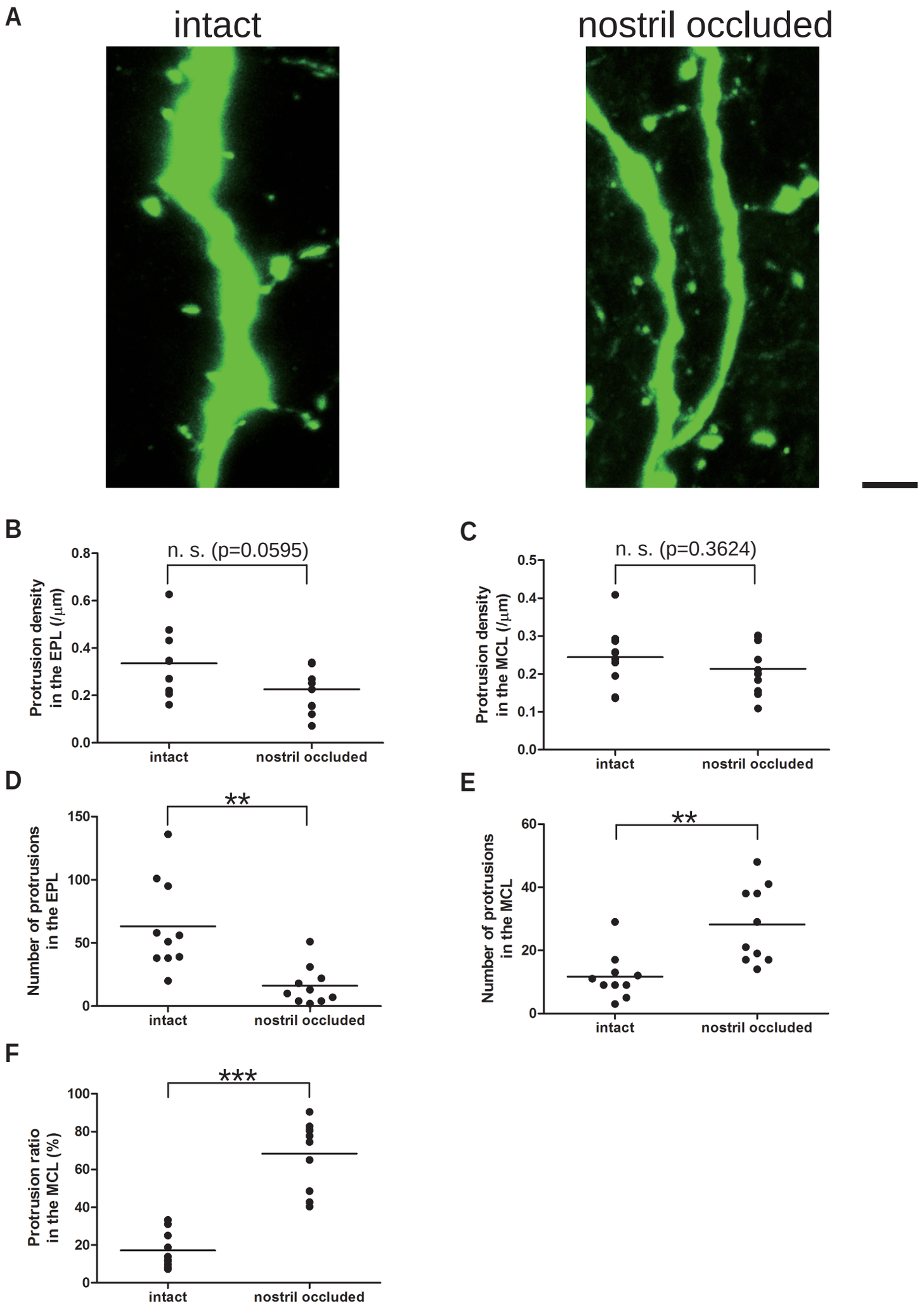
A
intact
nostril occluded
B
n. s. (p=0.0595)
Protrusion density in the EPL (/μm)
0.0
0.2
0.4
0.6
0.8
intact
nostril occluded
C
n. s. (p=0.3624)
Protrusion density in the MCL (/μm)
0.0
0.1
0.2
0.3
0.4
0.5
intact
nostril occluded
D
**
Number of protrusions in the EPL
0
50
100
150
intact
nostril occluded
E
**
Number of protrusions in the MCL
0
20
40
60
intact
nostril occluded
F
***
Protrusion ratio in the MCL (%)
0
20
40
60
80
100
intact
nostril occluded

Figure 13

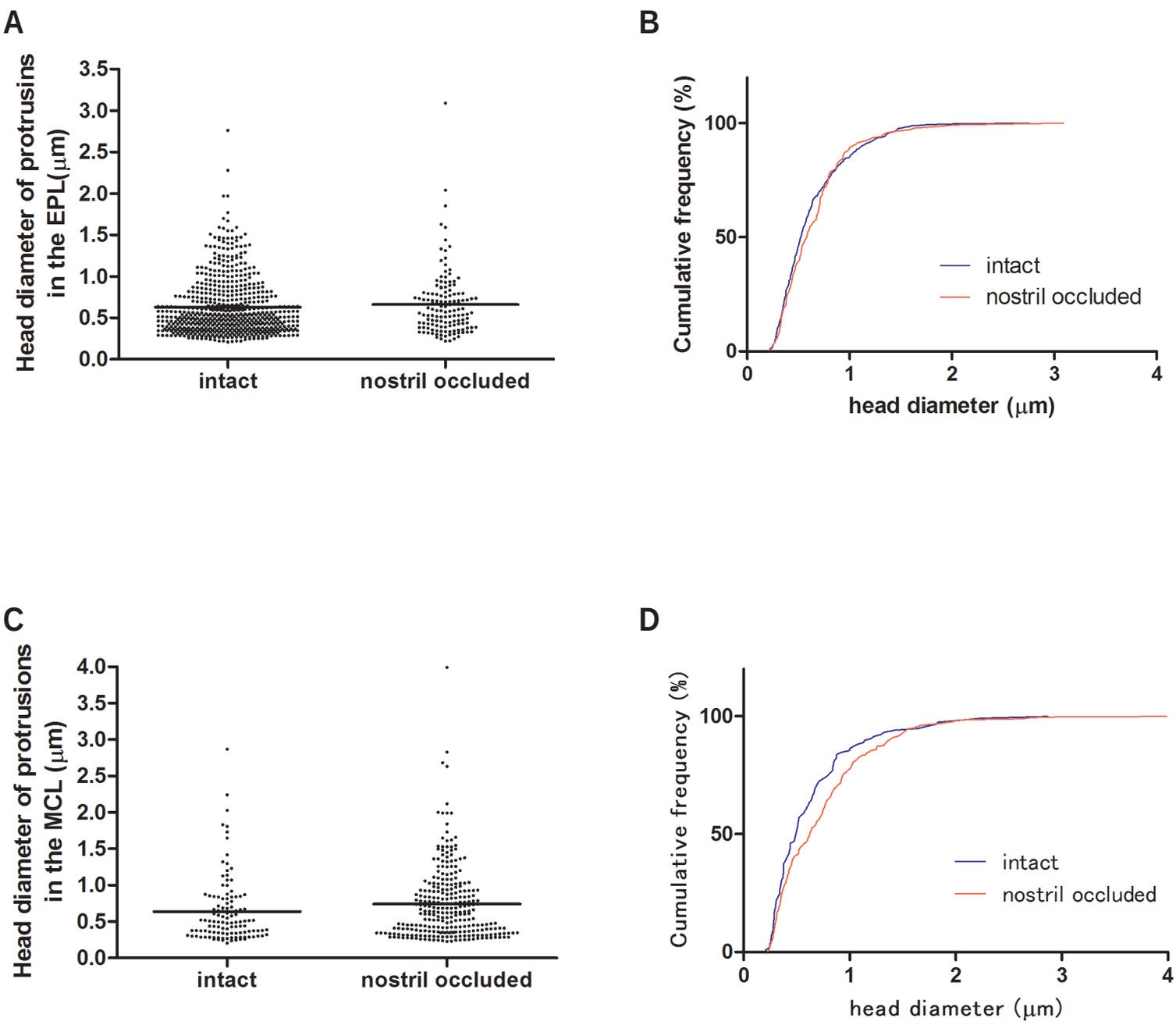
A
Head diameter of protrusins in the EPL(μm)
3.5
3.0
2.5
2.0
1.5
1.0
0.5
0.0
intact
nostril occluded
B
Cumulative frequency (%)
100
50
0
0
1
2
3
4
head diameter (μm)
intact
nostril occluded
C
Head diameter of protrusions in the MCL (μm)
4.0
3.5
3.0
2.5
2.0
1.5
1.0
0.5
0.0
intact
nostril occluded
D
Cumulative frequency (%)
100
50
0
0
1
2
3
4
head diameter (μm)
intact
nostril occluded